

TWO-DIMENSIONAL SEPARATE-SIDED
SURFACE HEIGHT PROFILING OF LUMBER

by

NATALIE IVONNE VADEBONCOEUR

B.Sc., University of Illinois at Urbana-Champaign, 2006

A THESIS SUBMITTED IN PARTIAL FULFILLMENT OF
THE REQUIREMENTS FOR THE DEGREE OF

MASTER OF APPLIED SCIENCE

in

THE FACULTY OF GRADUATE STUDIES

(Mechanical Engineering)

THE UNIVERSITY OF BRITISH COLUMBIA

(Vancouver)

April 2008

© Natalie Ivonne Vadeboncoeur, 2008

Abstract

Raw material accounts for a large proportion (approximately 75 percent) of a sawmill's operating costs. However, about 15 percent of raw material ends up as low valued sawdust and planer shavings due to inaccurate cutting. Sizable financial benefits can be realized through maximizing conversion of raw material into valuable solid wood. Advanced process control in a sawmill can help achieve straighter cuts closer to final product dimensions and reduce loss of valuable raw material. A novel and practical method for enhanced process control in a sawmill is presented. A laser arrangement consisting of industrial point and line scanners is used to obtain a surface profile of the entire (two-dimensional) top and bottom surfaces of a lumber board. Each surface profile is independent of the other and free of data contamination caused by relative motions between the measured surface and sensors. Point scanners and line scanners simultaneously record 1-D and 2-D height data, respectively, along the length of the board. One-dimensional height data are used to identify relative motions through a mathematical technique based on linear inverse theory. Subtracting relative motion information from raw line scanner data provides an accurate 2-D surface profile. A second line scanner placed below the board can be used to obtain a separate 2-D profile of the bottom lumber surface. Separate-sided profiling is advantageous because typically a different saw or machine mills each side of a board. Thus, knowing the surface profile of each side of a board is crucial not only in diagnosing a deficiency in the milling process but also in determining the location of this deficiency. Results demonstrate that two-dimensional surface profiling can identify common surface defects such as step, washboard and knot tear-out with an accuracy of 0.3mm. Reproduction of each surface is rapid (approximately 0.2 seconds) and stable.

Table of Contents

Abstract	ii
Table of Contents	iii
List of Figures	v
List of Symbols and Abbreviations	vii
Acknowledgments	ix
Chapter 1 Introduction and Background	1
1.1 Motivation	1
1.2 Challenge	1
1.3 Previous Work Done	2
1.4 Objectives	7
1.5 Overview	8
Chapter 2 Removal of Rigid-Body Motions	10
2.1 Introduction	10
2.2 Manageable Data	10
2.3 Identifying Rigid-Body Motions	12
2.3.1 Parallel-Sided Profiling with 6 Point Sensors	12
2.3.2 Solving the Inverse Problem	15
2.3.3 Reduced Equations	18
2.3.4 End-to-End Rigid-Body Motions	21
2.4 Removal of Rigid-Body Motions	25
2.5 Parallel-Sided Profiling with 8 Point Sensors	26
2.6 Double-Sided 2-D Surface Profiling	32
2.7 Regularization and Smoothing	34
Chapter 3 Experiment	38
3.1 Experimental Set-Up	38
3.2 Six Sensors Versus Eight Sensors	41
3.3 Removal of Rigid-Body Motions	45
3.4 Identifying 2-D Surface Features	52
Chapter 4 Conclusions	54
4.1 Summary of Results	54

4.2 Industrial Implementation	55
4.3 Limitations	56
4.4 Future Work	57
References	58

List of Figures

Figure 1	Four sensors arrangement for single-sided measurement	6
Figure 2	Replace point lasers in Figure 1 with line lasers	11
Figure 3	Three rigid-body motions detected by line scanner	12
Figure 4	Parallel-sided profiling arrangement using six sensors	13
Figure 5	Physical representation of second null vector	17
Figure 6	Order of equation combination for bandwidth minimization	19
Figure 7	2-D single-sided surface profiling arrangement	22
Figure 8	Identifying u-line and v-line in line scanner	26
Figure 9	2-D surface profiling with eight sensors	27
Figure 10	Order of equation combination for bandwidth minimization using eight sensors	29
Figure 11	Double-sided 2-D surface profiling arrangement	33
Figure 12	Thickness measurement using double-sided 2-D line scanners	34
Figure 13	Experimental set-up; 8 point sensors and 2 line sensors	38
Figure 14	Close-up front view of all top sensors; Sensors ABCD behind EFGH	39
Figure 15	6 Sensor 1-D parallel profiles of top surface of sinusoidal board – no regularization	42
Figure 16	8 Sensor 1-D parallel profiles of top surface of sinusoidal board – no regularization	43
Figure 17	6 Sensor parallel 1-D profiles of top surface of sinusoidal board – with regularization: $\alpha_{flat}=0.1$, $\alpha_{smooth}=1.0$	44
Figure 18	8 Sensor parallel 1-D profiles of top surface of sinusoidal board – with regularization: $\alpha_{flat}=0.1$, $\alpha_{smooth}=1.0$	44
Figure 19	Step placed on center 4 rollers to introduce known translation	45

Figure 20	Raw 2-D data for flat board with translational rigid-body motion	46
Figure 21	Raw 1-D data for flat board with translational rigid-body motion	47
Figure 22	Translation of flat board with step placed on center rollers	47
Figure 23	2-D plot of flat board with translation removed	48
Figure 24	Comparison of 1-D u profile and 2-D u -line profile for flat board	48
Figure 25	Comparison of 1-D v profile and 2-D v -line profile for flat board	49
Figure 26	Raw 2-D data for upside-down sinusoidal board	49
Figure 27	Translation and roll of upside-down snake board	50
Figure 28	Corrected 2-D plot of bottom surface of sinusoidal board	50
Figure 29	Comparison of 1-D u profile and 2-D u -line profile for upside-down sine board	51
Figure 30	Comparison of 1-D v profile and 2-D v -line profile for upside-down sine board	51
Figure 31	Surface with band saw washboard and 5mm bow	52
Figure 32	2"x6" with approximately 1mm step running down center of board	53
Figure 33	2"x10" with scallop defect and knot tear-out	53

List of Symbols and Abbreviations

A, B, C, D, E, F, G, H	sensors
$a_i, b_i, c_i, d_i, e_i, f_i, g_i, h_i$	sensor data
H	arbitrary point from which surface height is measured
i, j	indices
$1-D, 2-D$	one-dimensional, two-dimensional
G	kernel matrix
$G^T G$	symmetrical banded matrix
m	model vector
M	total number of unknowns
d^{obs}	observed data vector
$misfit$	data misfit
n	total number of profile points
n_m	total number of measurements ($n-2l$) from each sensor
u, v	1-D parallel surface profiles
w	translation
y	roll
z	pitch
α, γ	height fractions of rotation for inner sensors
p, q, r, s	sensor spacings
l	half of sensor span
x	distance from surface start point to sensor A
u -line	sensors $ABCD$ for 8-sensor setup
v -line	sensors $EFGH$ for 8-sensor setup
$slope$	slope of board during roll
d	distance between u -line and v -line
j	horizontal distance ($p+q-r$) between sensors C and F
k	horizontal distance ($q+r-p$) between sensors B and G
L	physical distance between line scanners
L_1, L_2	distance from first and second line scanners to board

$raynum_{max}$	max ray number in line scanner
b_k	binomial smoothing coefficient
N_p	any integer
κ	curvature
MCO	mid-chord offset
ACO	asymmetric chord offset
$\alpha_{small}, \alpha_{flat}, \alpha_{smooth}$	penalty weight
$W_{small}, W_{flat}, W_{smooth}$	0 th , 1 st , 2 nd order derivative operators
I	identity matrix
β	regularization parameter
h	measurement increment
σ	data standard deviation
N	total number of data points

Acknowledgements

I sincerely thank my advisor Dr. Gary Schajer for his guidance and financial support throughout my research work at UBC. I had a wonderful educational experience thanks to his wisdom and generosity.

I am truly grateful for my husband's guidance and constant support not only throughout this thesis but in life, sport and school. His self-discipline and determination in everything he does has inspired me to chase my dreams and never settle for less. His constant encouragement has given me the confidence to do so.

Chapter 1: Introduction and Background

1.1 Motivation

Sawmills can realize sizable benefits through savings in raw material. A one percent reduction in the amount of solid wood lost to sawdust in one year results in an additional profit of approximately \$320,000 for a mill producing 100 million board-feet of lumber annually [1]. This is because about 75 percent of a sawmill's operating costs are accounted for by raw material alone [2]. Small gains in raw material, thus, equate to large financial savings.

Improvements in sawmill process control can reduce wasted raw material. Lumber boards are initially sawn oversized to allow for inaccuracies that occur in the secondary breakdown, the process by which a cant is reduced into lumber boards. These inaccuracies result from anything from dull saw blades to inaccurate feed rates of the cant [3]. At the end of the milling process, the boards are planed to target dimensions. Better control over the performance of various mechanisms in the milling process results in boards being sawn with less variation [3]. This allows boards to be sawn closer to target dimensions in the primary breakdown, thereby reducing the amount of valuable raw material lost in planing.

1.2 Challenge

Typically, a sawmill conducts quality control checks by taking approximately six to ten thickness measurements of lumber boards using calipers [4]. This is slow and provides little information about the overall shape of each surface of the board. Common surface defects such as washboard and step (mismatched surface heights) are unlikely to be identified with thickness measurements alone. The same problem exists for on-line thickness measuring

where a complete thickness profile of each board is obtained. This process is much faster and allows many more boards to be measured but again does not allow for recognition of the shape of each separate lumber surface. A different saw or machine typically mills each side of a board. Thus, knowing the location of a surface defect on the board indicates which machine or component needs adjustment.

On-line surface height profiling, as opposed to thickness profiling, provides a more complete picture of the overall shapes of both top and bottom surfaces of a board in real time [5]. This facilitates faster, more accurate identification of particular surface defects that point to specific problems in the milling process. These problems can then be adjusted immediately, thereby reducing the amount of defective material produced.

The challenge lies in measuring accurate separate-sided surface profiles on-line in spite of unavoidable rigid-body motions of each board as it travels along a conveyor in the sawmill. These rigid-body motions include translation and rotation (both pitch and roll) and register as false height readings when they occur during measurement. In order to obtain an accurate surface profile, it is necessary to remove these false height readings from the raw data.

1.3 Previous Work Done

Surface profiling has played an important role as an inspection technique in many different fields and applications ranging in scale from nanometer to kilometer. Many researchers have been interested in absolute height of the surface being observed, be it of an optical lens [6], a railway [7] or the Earth [8]. Regardless of scale, obtaining accurate measurements of any surface requires a complete lack of relative motion between a sensor

and its target. Scanning electron microscopes produce excellent topographic maps in measuring thin film surfaces [6], as do stylus-based profilometers in measuring closure deformation of rock joints [9]. In each instance the specimen is fixed and the sensor's movement is precisely controlled. In the case of on-line lumber surface profiling with a fixed sensor, achieving zero relative motion is impossible due to rigid-body motions experienced by the board as it is transported along a series of conveyers. Several applications of surface profiling, in spite of relative motion between the sensor and target, are discussed below.

Interferometric synthetic aperture radar (InSAR) is an example of two-dimensional surface profiling used to produce digital elevation models (DEMs) of the Earth's surface primarily for analyzing and interpreting tectonic and volcanic activity [10]. This is a form of active remote sensing in which dual antennas aboard an aircraft emit radiation that is reflected back from the target. Phase shift between outgoing and incoming signals is accurately measured and reflects the distance between the signal emitter and target. Height data can then be extracted.

In the case of topographic mapping mobile sensors measure a fixed target. Thus, pitch and roll of the aircraft must be accounted for as to not disrupt measurement accuracy of the terrain below. This is attempted by considering both antennae to be rigidly connected [11]. Relative motion is then considered to be the same at each sensor and can be cancelled out.

While it is much more practical in a mill to use fixed sensors capable of scanning a mobile lumber surface, a basic principle of motion compensation can be taken from topographic mapping using InSAR. This principle involves the use of multiple sensors to distinguish between surface features and relative motions.

A multi-sensor arrangement was employed in a series of studies involving one-dimensional surface height profiling of both roads [12, 13] and railways [14, 15, 7] for corrugation detection. The method commonly used in each study involves taking local curvature measurements of the surface using multiple sensors mounted on a vehicle traversing the terrain being measured. Thus, relative motion exists between the sensors and surface during measurement due to vibrations and wheel irregularities while the vehicle is in motion. The sensors are considered rigidly connected allowing the assumption that relative motion is the same at each sensor. Relative motion can then be eliminated mathematically. Curvature information is double integrated to obtain surface height.

Curvature is estimated using the second finite difference approximation shown below.

$$\kappa(i) \cong \frac{2f_i - f_{i-1} - f_{i+1}}{h^2} = -\frac{2MCO}{h^2}$$

where MCO is the three-point mid-chord offset and is calculated as follows:

$$MCO = \frac{a - 2b + c}{2}$$

where a , b and c represent raw data from three in-line equally spaced sensors with total sensor span, or chord length, h . The chord length is also considered the discretization step length.

Curvature integration as a method for profiling lumber has several drawbacks [16]. First, high frequency surface variation tends to go undetected due to the large spacing between sensors. Second, complete attenuation of certain wavelengths occurs when there exists a common factor between the wavelength and sensor spacing. Third, MCO measurement accuracy is insufficient to resolve wavelengths longer than

$$\lambda_{\max} = 2h\sqrt{\frac{U}{\sigma}}$$

where h is chord length (sensor span), U is the surface profile amplitude and σ is the standard deviation of measurement noise [17]. The data do not provide a geometrical relationship between sequential measurements that would aid in detection of longer wavelengths. This is because it is not stored for a later calculation. Rather, the data is received and used instantaneously to compute curvature. This also does not allow for data averaging that can aid in noise reduction.

Corbin [7] discusses a method for identifying both short and long wavelengths using curvature integration. He employs an asymmetrical array of sensors that combine to form an asymmetric-chord offset (*ACO*). He mathematically converts a set of sequential *ACO* measurements into *MCO* data for three equidistant sensors arranged one unit apart. The wide sensor spacing allows for longer wavelength detection with the sequential measurements aiding in smaller wavelength detection. His solution, however, is non-unique [16].

An *inertial method* involving the use of accelerometers has also been applied to detect railway corrugations [18]. While this method allows for data averaging it also requires constant contact between the sensor and surface, an impossible requirement for lumber surface profiling.

Gazzarri and Schajer [19] have developed a method for one-dimensional profiling of lumber boards that addresses the drawbacks of curvature integration. The work presented in this thesis is largely based on this method. They discuss several different arrangements of multiple laser range sensors that are able to profile either one or two sides of a lumber board simultaneously or detect board twist. All sensors are synchronized and take sequential measurements along the length of a passing board. This method is based on the observation that during profiling, surface features of a lumber board appear in delayed sequence among

fixed multiple sensors while rigid-body motions of the board appear simultaneously. It is this observation that allows for the mathematical separation of rigid-body motions from raw sensor data leaving an accurate one-dimensional profile.

In single-sided measuring four sensors are required as shown in Figure 1 below. Translation and rotation of the board combine with surface heights as follows:

$$\begin{aligned}
 a_i &= u_i & + w_i - z_i(-l)/l \\
 b_i &= u_{i+p} & + w_i - z_i(p-l)/l \\
 c_i &= u_{i+p+q} & + w_i - z_i(p+q-l)/l \\
 d_i &= u_{i+p+q+r} & + w_i - z_i(p+q+r-l)/l
 \end{aligned} \tag{1}$$

where a , b , c , and d are “height” data from each sensor, u is the surface profile, w is translation, z is rotation and l is half the sensor span, $(p+q+r)/2$. The spacing between sensors a and b is p , b and c is q , and c and d is r . These spacings must contain no common factors as to prevent attenuation of any wavelength.

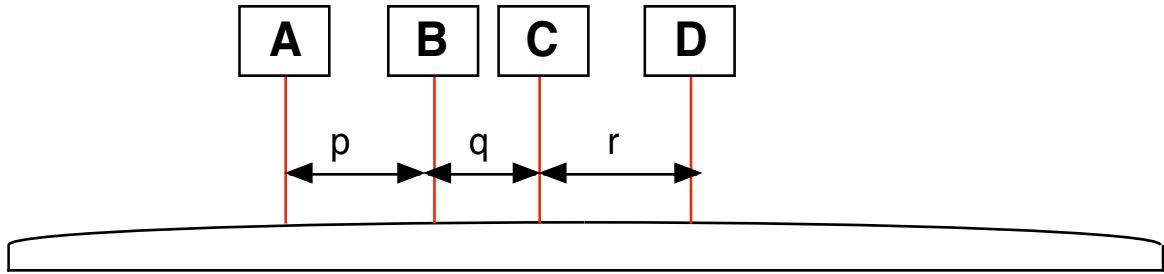


Figure 1: Four sensors arrangement for single-sided measurement

While sensor data a_i , b_i , c_i , and d_i are known; the surface profile (u) and rigid-body motion components (w , z) of the data are unknown. In order to obtain the surface profile from equation (1) a matrix inversion must take place. Thus, the equations in (1) are characterized as linear inverse equations. Inverse equations are typically ill-posed and, thus, highly sensitive to noise in the data. Schajer and Gazzarri [17] reduce noise with data averaging.

Equation (1) can accommodate additional sensors for more complex measurement. For example, six sensors, three on top and three on bottom, are necessary to perform double-sided surface profiling [20]. Both profiles are completely independent of one another. Parallel-sided profiling employs two parallel rows of three sensors on one side of the board. This arrangement is able to detect both physical and rigid twist of the board in addition to translation and rotation [20].

One-dimensional profiling is successful in producing accurate separate-sided profiles in the presence of rigid-body motions [20]. However, two-dimensional surface roughness patterns as well as features such as knot tear-out that do not fall in the line of measurement are undetectable. Detection of these features would help diagnose problems in the milling process. Therefore, expanding this measurement to cover the entire surface of the board is highly desirable with respect to better process control.

1.4 Objectives

Two-dimensional surface height profiling can provide a complete picture of the entire surface, both top and bottom, of a board. Measurements are taken along the width and length of each surface, rather than just the length as in one-dimensional profiling. The major challenge, however, lies in managing copious amounts of data presented when using line lasers instead of point lasers to capture two-dimensional measurements. Feeding this amount of data into an algorithm that separates rigid-body motions from the raw data slows down the calculation making it impractical to identify problems in the milling process in real time. The work presented in this thesis deals with identifying accurate, separate-sided two-dimensional

surface height profiles of lumber boards in a time frame practical for keeping up with production speed.

A combination of line and point lasers is used to achieve the above objective. Two line lasers, one positioned above and below the conveyor, record two-dimensional surface height data as each board passes. This data is contaminated with false height readings due to rigid-body motions of the board during passing. An array of point lasers synchronized with the line lasers is responsible for identifying the amplitude of each rigid-body motion as done in the one-dimensional profiling method. An algorithm is used to subtract the amplitude of each rigid-body motion from the raw two-dimensional data. What remains is an accurate representation of a lumber board surface independent of any other surfaces.

1.5 Overview

The present work is organized as follows: Chapter 2 contains a discussion about the method behind obtaining accurate separate-sided 2-D surface height profiles in a practical time frame for industrial implementation. The mathematical background for identifying rigid-body motions using the proposed arrangement of point and line sensors as well as the method for removal of rigid-body motions from 2-D data are explained. Smoothing techniques as a means to reduce noise amplification in the solution are also discussed.

Chapter 3 provides a detailed explanation of the experimental work that verifies the method discussed in Chapter 2. The experimental set-up is explained. Demonstrations of the performance of two different sensor arrangements are presented as well as demonstrations of rigid-body motion removal. Results of boards containing surface features of industrial interest with respect to sawmill process control are also given.

Chapter 4 contains a summary of results and an overall assessment of the contributions and limitations of the research work presented. Recommendations for future work are discussed here as well.

Chapter 2: Removal of Rigid-Body Motions

2.1 Introduction

There are three main objectives of the following research. First, a 2-D surface height profile is to be determined for one surface of the board independent of the other. Second, an accurate two-dimensional (2-D) surface height profile of a lumber board that is free of contamination from false height readings caused by rigid-body motions during measurement is to be determined. Third, calculation time must be to keep up with sawmill production speed.

The proposed method involves the use of an arrangement of synchronized point and line lasers. Each laser performs sequential measurements of a passing board. The point lasers are arranged in the parallel-sided profiling configuration developed by Gazzarri [16]. They record one-dimensional (1-D) surface height data, while line lasers record 2-D surface height data. The 1-D data are used to detect the amplitude of rigid-body motions. This is done based on the fundamental idea that rigid-body motions of a passing board appear simultaneously among multiple point lasers, while surface features appear in delayed sequence [16]. This allows for mathematical separation of rigid-body motions that can then be removed from the 2-D surface height data detected by the line laser. What remains is an accurate 2-D surface profile free of rigid-body motion contamination.

2.2 Manageable Data

Theoretically, one can obtain an accurate 2-D surface profile by simply replacing each point laser in the four-sensor arrangement discussed in Section 1.3 (See Figure 1) with a line laser measuring across the width of the board as shown in Figure 2. This is because a line

scanner is essentially a row of many closely spaced point lasers. The 1-D profiling algorithm could then be applied to each “point” in the line scanner data along the length of the board providing many 1-D profiles across the width of the board. Interpolating between these 1-D profiles creates a complete 2-D surface profile.

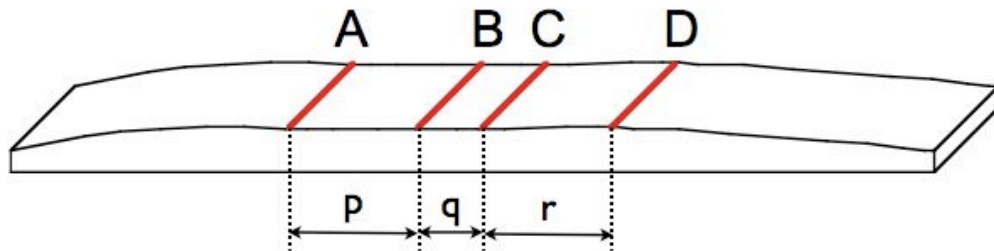


Figure 2: Replace point lasers in Figure 1 with line lasers

Replacing point lasers with line lasers is a conceptually simple approach to 2-D profiling given that the algorithm for 1-D profiling has already been established. However, the time required to calculate a 1-D profile for each point in a line scan compromises the system’s ability to operate quickly. This is due to the large quantity of data presented by a single line scanner.

In order to reduce the amount of data required to obtain a 2-D profile, a system comprised of both point and line lasers is employed. Point laser data are involved in the 1-D profiling inverse calculation in order to extract rigid-body motion information. This differs from 1-D profiling where the focus was on extracting 1-D surface height profiles from point laser data. The line scanner (2-D) data is not involved in the inverse calculation. Instead, rigid-body motion information determined by point lasers is removed from the 2-D data. This arrangement allows fast calculation speeds because a manageable amount of data is used in the calculation.

Further explanation of the rigid-body motion calculation follows as well as discussion of several different arrangements of point and line lasers.

2.3 Identifying Rigid-Body Motions

Three different rigid-body motions of a lumber board can register as false surface height readings in a 2-D scan. These include translation, rotation about the y -axis (pitch) and rotation about the x -axis (roll). Figure 3 illustrates these three rigid-body motions relative to a line scanner represented by the red line. It is necessary to be able to identify the magnitude of each of these rigid-body motions in order to remove this information from the 2-D scanner data. The parallel-sided profiling arrangement discussed by Schajer and Gazzarri [20] is capable of identifying all three rigid-body motions.

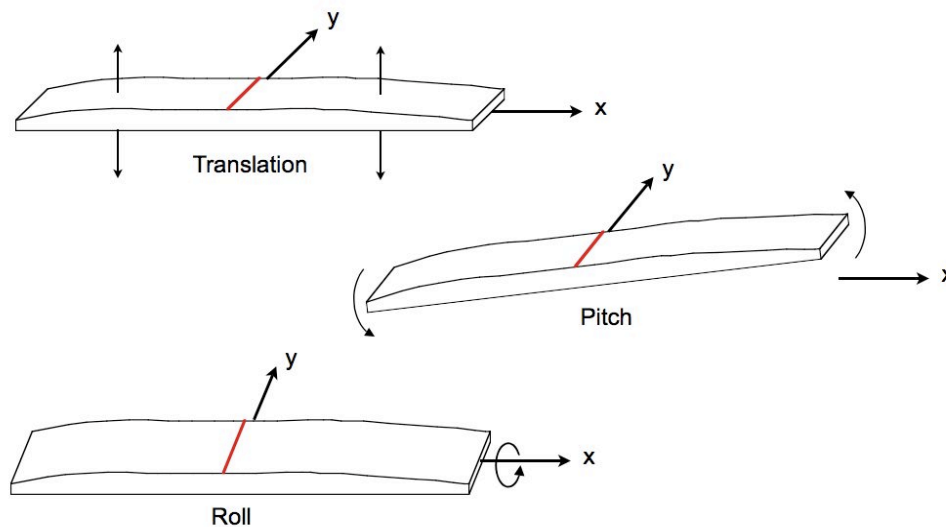


Figure 3: Three rigid-body motions detected by line scanner

2.3.1 Parallel-Sided Profiling with 6 Point Sensors

One-dimensional profiling using four sensors (see Figure 1) can be expanded to see more of the lumber surface [16]. Two parallel lines of three point sensors each, as shown in

Figure 4, reveal board twist as well as the 1-D profiles along two lines on one surface of the board. Additionally, this arrangement is capable of identifying translation, pitch and roll making it suitable for 2-D surface profiling. An overview of the mathematical background behind 1-D surface profiling developed by Gazzarri [16] as it relates to a parallel-sided arrangement of sensors follows.

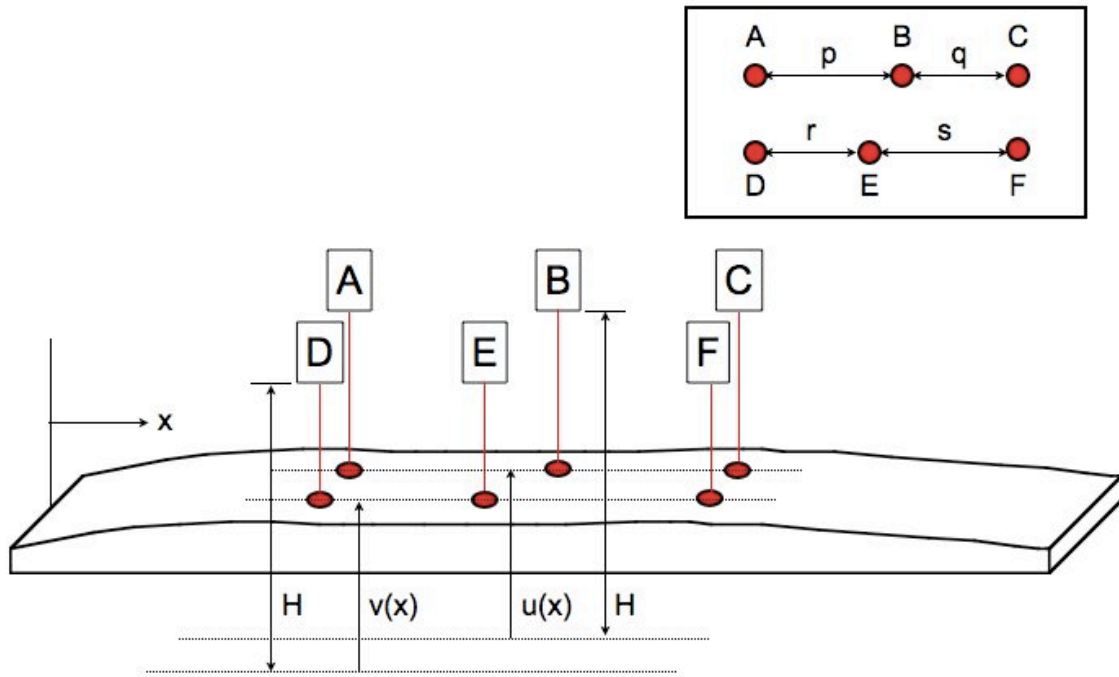


Figure 4: Parallel-sided profiling arrangement using six sensors

Each point scanner measures the distance from sensor to board surface. This data is inverted in Equation (2) to reflect surface height [16].

$$a(x) = H - a^*(x) \quad (2)$$

where $a(x)$ is the inverted surface height as measured by sensor A , H is an arbitrary reference point below the board surface, $a^*(x)$ is the distance from sensor A to the surface and x is the horizontal position along the board at which a height measurement is taken. When measuring a single surface, the exact value of H is not critical [16].

Middle sensors B and E are offset as to maintain an asymmetry in the arrangement and widen the spectrum of wavelengths able to be identified. This is explained in further detail in section 2.3.2. It is important to maintain a smaller spacing between the middle sensors because it improves the system's ability to detect curvature [16].

Data from each sensor consists of a surface height quantity as well as false height readings from three rigid-body motions. The sensor equations developed by Gazzarri [16] accompanying this arrangement reflect this combination and are shown below in Equations (3).

$$\begin{aligned}
 a(x) &= u(x) & + w(x) & + y(x) & - z(x) \cdot (-l)/l \\
 b(x) &= u(x+p) & + w(x) & + y(x) & - z(x) \cdot (p-l)/l \\
 c(x) &= u(x+p+q) & + w(x) & + y(x) & - z(x) \cdot (p+q-l)/l \\
 d(x) &= v(x) & + w(x) & - y(x) & - z(x) \cdot (-l)/l \\
 e(x) &= v(x+r) & + w(x) & - y(x) & - z(x) \cdot (r-l)/l \\
 f(x) &= v(x+r+s) & + w(x) & - y(x) & - z(x) \cdot (r+s-l)/l
 \end{aligned} \tag{3}$$

$a(x), b(x), c(x), d(x), e(x), f(x) \equiv$ sensor data

$u(x), v(x) \equiv$ parallel 1-D surface height profiles

$w(x) \equiv$ translation

$z(x) \equiv$ rotation about y-axis (pitch)

$y(x) \equiv$ rotation about x-axis (roll)

$p, q, r, s \equiv$ sensor spacing

$l \equiv$ half of sensor span = $(p+q)/2 = (r+s)/2$

All rigid-body motions are measures of height. Pitch is measured about the center of the sensor span and roll is measured about the center of the two parallel lines of sensors.

The variable x represents space and time in Equation (3) [16]. When associated with surface heights u and v it marks the corresponding position along the length of the board. It can be seen that surface features u and v are delayed by the spacing between each sensor, not by the time it takes for the surface feature to arrive at the next sensor. This eliminates the requirement that the board travel at a known constant speed during measurement. In terms of rigid-body motions w , y , and z , x represents the point in time when each motion occurs. This allows each motion to be linked with its corresponding sensor measurement. Thus, accurate elimination of rigid-body motion from sensor data can occur.

2.3.2 Solving the Inverse Problem

Given surface profiles u and v and corresponding rigid-body motions in Equations (3), the *forward calculation* produces data for each sensor. However, the sensor data in surface profiling are known, while the variables u , v , w , y , and z represent unknowns. The process of solving for each variable requires an inversion of the equation set, classifying Equations (3) as an *inverse problem* [21]. Inverse equations have a variety of associated challenges. They are typically ill-posed and can produce a non-unique solution. Under these conditions small variances in data such as noise are amplified in the solution [21]. Several techniques for dealing with these challenges as they pertain to surface profiling are discussed.

One-dimensional surface measurement begins when all six sensors detect the board surface. As the board advances on a conveyor each sensor takes sequential measurements at specified distance intervals until the end of the board reaches the group of sensors. The number of measurements taken is, thus,

$$n_m = n - p - q \quad (4)$$

where n is the total number of surface points. Equations (5) reflect measurement, as they are a discrete representation of Equations (3).

$$\begin{aligned}
a_i &= u_i + w_i + y_i - z_i(-l)/l \\
b_i &= u_{i+p} + w_i + y_i - z_i(p-l)/l \\
c_i &= u_{i+p+q} + w_i + y_i - z_i(p+q-l)/l \\
d_i &= v_i + w_i - y_i - z_i(-l)/l \\
e_i &= v_{i+q} + w_i - y_i - z_i(r-l)/l \\
f_i &= v_{i+q+p} + w_i - y_i - z_i(r+s-l)/l
\end{aligned} \quad 1 \leq i \leq n_m \quad (5)$$

Equations (5) can be expressed in matrix form as shown in Equation (6) [21].

$$G \cdot m = d^{obs} \quad (6)$$

where G contains the coefficient of each variable on the right-hand side of equations (5) and is called the *kernel* matrix. The model vector m contains all values of u , v , w , y , and z and the data from each sensor is contained in vector d^{obs} .

For the simple case in which there are $n = 20$ surface points and sensor spacings are as follows: $p = 3$, $q = 2$, $r = q$, and $s = p$, the size of m (number of unknowns) is $2 \cdot n + 3 \cdot n_m = 85$ and d (number of knowns) is $6 \cdot n_m = 90$. The excess data beyond the number of unknowns indicates that this is an over-determined system. In order to obtain a solution for equation (6) it is necessary for the number of knowns to equal or exceed the number of unknowns. Therefore, a board that is at least three times the length of the sensor span must be scanned in order to realize a solution. This calculation is shown in (7).

$$\begin{aligned}
&knowns \geq unknowns \\
&6 \cdot n_m \geq 2 \cdot n + 3 \cdot n_m \\
&6 \cdot (n - p - q) \geq 2 \cdot n + 3 \cdot (n - p - q) \\
&n \geq 3(p + q)
\end{aligned} \quad (7)$$

Kernel matrix G must be inverted in order to solve for the model vector. However, G is not full-rank in columns due to the existence of two separate null vectors that when multiplied by G produce a zero data vector d^{obs} [16]. The first null vector results from a lack of defined boundary conditions for the system. A uniform height change could be interpreted as a rigid-body motion. To eliminate this ambiguity, three points are needed to define the board surface's position in space. The first values of both surface profiles (u_1 and v_1) and the last value of one surface profile (u_n or v_n) are set to zero. Each successive profile value for both parallel lines is then built on this defined position. Not defining a fourth value allows the end of one profile to “float” freely revealing board twist.

Sensor spacings must be chosen carefully in order to avoid the second null vector. Consider the case illustrated in Figure 5 where a board has a sinusoidal surface shape of period p and is undergoing a sinusoidal translation with the same amplitude and wavelength as the surface shape but opposite phase. If all sensors were spaced evenly ($p=q=r=s$) surface shape would be indistinguishable from rigid-body motion in the sensor data. Ensuring that there are no common factors between sensor spacings eliminates the second null vector [7].

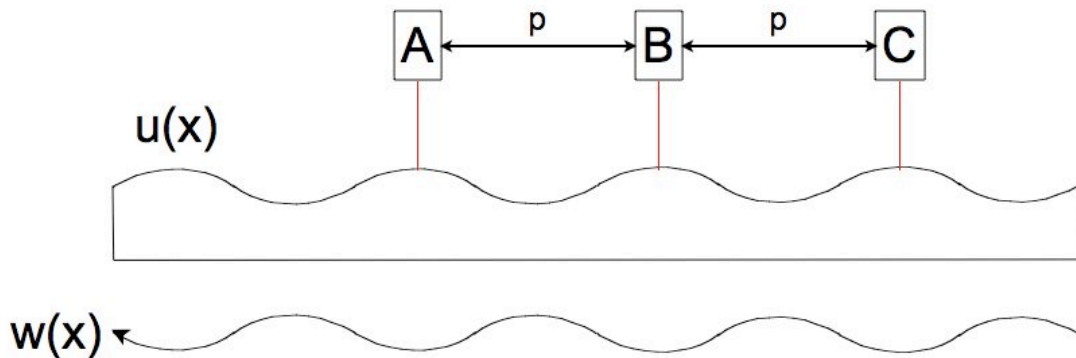


Figure 5: Physical representation of second null vector

Having accounted for both null vectors and ensured that there are at least $3(p+q)$ data, the inverse problem can be solved. For the case when the number of data exceeds the number of unknowns, the kernel G is a rectangular matrix. A least-squares model that minimizes the *misfit*, or difference, between observed and predicted data is used [21].

$$misfit = d^{obs} - G \cdot m \quad (8)$$

The Euclidian norm is a commonly used measure of the misfit and is defined as the square root of the inner product of a vector x with itself:

$$\|x\|_2 = \sqrt{x^T x} \quad (9)$$

The minimization of the misfit norm is then represented by the least squares approximation:

$$\min \|G \cdot m - d^{obs}\|^2 \quad (10)$$

Differentiating equation (10) with respect to m and setting it equal to zero provides the *normal equations* (11) that are used in this over-determined surface profiling problem [21].

$$G^T G \cdot m = G^T \cdot d^{obs} \quad (11)$$

The model vector m is then determined by multiplying each side of equation (11) by the inverse of $G^T G$ as shown in equation (12).

$$m = (G^T G)^{-1} G^T \cdot d^{obs} \quad (12)$$

$G^T G$ is a symmetrical banded matrix that can be solved using a specialized symmetrical banded solver in order to reduce calculation time.

2.3.3 Reduced Equations

It can be seen from the example given in section 2.3.1 that the kernel matrix for parallel-sided profiling is large even for a simple case containing 20 surface points. (A full-sized lumber board will typically contain 800 to 1000 surface points.) For a banded matrix G the time required for an inverse calculation is proportional to the square of the number of

surface points. To reduce calculation time, it is desirable to maintain a small kernel matrix given the length of the board. Minimizing inverse calculation time is especially desirable for 2-D as opposed to 1-D surface profiling. The extra step present in 2-D profiling in which rigid-body motions are removed from 2-D data adds time to the calculation. Therefore, a reduced form of equation set (5) is discussed.

Equations (5) can be combined and manipulated to eliminate rigid-body motions w , y , and z leaving three equations in terms of u and v only. This greatly reduces the size of the kernel matrix and hence the calculation time. Solving for rigid-body motions can be done rapidly with further matrix solution after u and v have been determined.

Roll (y) can quickly be eliminated from equations (5) by simply combining the first three and last three equations. It is important to follow the specific order shown in Figure 6 when combining equations (5). This order ensures that each equation for a particular sensor is combined with the equations of its closest sensors on the opposite parallel line. This maintains a minimal bandwidth in the $G^T G$ matrix and further contributes to a faster calculation. The method for eliminating y is presented symbolically in (13). Each sensor equation is assigned a number in parenthesis. New equations formed by combining original equations are assigned numbers above 6. These numbers do not correspond to the numbered equations throughout the text.

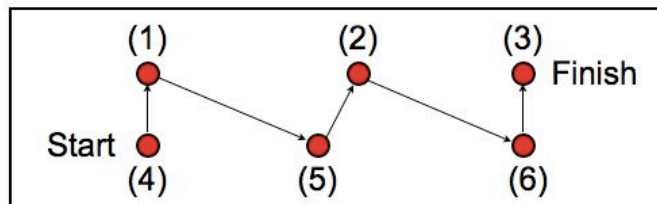


Figure 6: Order of equation combination for bandwidth minimization

$$\begin{aligned}
(1) \quad a_i &= u_i + w_i + y_i - z_i(-l)/l \\
(2) \quad b_i &= u_{i+p} + w_i + y_i - z_i(p-l)/l \\
(3) \quad c_i &= u_{i+p+q} + w_i + y_i - z_i(p+q-l)/l \\
(4) \quad d_i &= v_i + w_i - y_i - z_i(-l)/l \\
(5) \quad e_i &= v_{i+q} + w_i - y_i - z_i(r-l)/l \\
(6) \quad f_i &= v_{i+q+p} + w_i - y_i - z_i(r+s-l)/l
\end{aligned} \tag{13}$$

$$(7) = (4) + (1)$$

$$(8) = (1) + (5)$$

$$(9) = (5) + (2)$$

$$(10) = (2) + (6)$$

$$(11) = (6) + (3)$$

The next variable that can be eliminated from equations (5) is translation (w). The process is as follows:

$$(12) = (7) - (8)$$

$$(13) = (8) - (9)$$

$$(14) = (9) - (10)$$

$$(15) = (10) - (11)$$

(14)

The final variable z corresponding to pitch can be eliminated as follows:

$$(16) = (1 + \alpha)(12) - (1 - \alpha)(13)$$

$$(17) = (13) - (14)$$

$$(18) = (1 - \alpha)(14) - (1 + \alpha)(15)$$

(15)

where α is $(p-q)/(p+q)$, the rotational height fraction for inner sensors B and E . Equations (15) are only in terms of 1-D profiles u and v . A new kernel matrix can be constructed from these equations. There are $2(n)$ unknowns and $3(n-p-q)$ knowns. Returning to the example given in section 2.3.2 in which $n=20$, $p=3$, $q=2$, $r=q$ and $s=p$; the dimensions of G are now 40×45 reducing the matrix to 1/5 of its “unreduced” size. Equations (15) are written out below.

$$\begin{aligned}
(-1 + \alpha)[A_i - B_i] + (1 + \alpha)[D_i - E_i] &= (-1 + \alpha)u_i + (1 + \alpha)v_i + (1 - \alpha)u_{i+p} - (1 + \alpha)v_{i+q} \\
A_i - B_i - E_i + F_i &= u_i - u_{i+p} - v_{i+q} + v_{i+q+p} \quad (16) \\
(-1 - \alpha)[B_i - C_i] + (1 - \alpha)[E_i - F_i] &= (1 - \alpha)v_{i+q} - (1 + \alpha)u_{i+p} + (1 + \alpha)u_{i+p+q} + (-1 + \alpha)v_{i+p+q}
\end{aligned}$$

The least squares minimization method described in the previous section is used to solve equations (16) for u and v .

Once profiles u and v have been calculated, they can be used to determine each rigid-body motion by substituting them back into equations (5). Equations (17) result from moving all knowns to the left side of equations (5) and all unknowns to the right.

$$\begin{aligned}
a_i - u_i &= w_i + y_i - z_i(-l)/l \\
b_i - u_{i+p} &= w_i + y_i - z_i(p-l)/l \\
c_i - u_{i+p+q} &= w_i + y_i - z_i(p+q-l)/l \\
d_i - v_i &= w_i - y_i - z_i(-l)/l \\
e_i - v_{i+q} &= w_i - y_i - z_i(r-l)/l \\
f_i - v_{i+q+p} &= w_i - y_i - z_i(r+s-l)/l
\end{aligned} \quad 1 \leq i \leq n_m \quad (17)$$

Least squares minimization is used to obtain three equations corresponding to each rigid-body motion as shown in (18). Since there are only three equations, they can be directly written into the computer program to facilitate faster calculation time. Solving equations (18) is a simple forward calculation.

$$\begin{aligned}
w_i &= \frac{1}{6}[(a_i - u_i) + (b_i - u_{i+p}) + (c_i - u_{i+p+q}) + (d_i - v_i) + (e_i - v_{i+q}) + (f_i - v_{i+q+p})] \\
z_i &= \frac{1}{4 + 12\alpha^2} [2(a_i - u_i) + (3\alpha - 1)(b_i - u_{i+p}) - (1 + 3\alpha)(c_i - u_{i+p+q}) + (1 + 3\alpha)(d_i - v_i) + (1 - 3\alpha)(e_i - v_{i+q}) - 2(f_i - v_{i+q+p})] \\
y_i &= \frac{1}{4 + 12\alpha^2} [2\alpha^2(a_i - u_i) + (1 - \alpha - 2\alpha^2)(b_i - u_{i+p}) + (1 + \alpha + 2\alpha^2)(c_i - u_{i+p+q}) - (1 + \alpha + 2\alpha^2)(d_i - v_i) - (1 - \alpha + 2\alpha^2)(e_i - v_{i+q}) - 2\alpha^2(f_i - v_{i+q+p})]
\end{aligned} \quad (18)$$

2.3.4 End-to-End Rigid-Body Motions

A line scanner is placed mid-span of the parallel-sided profiling arrangement, as shown in Figure 7 for single-sided 2-D profiling. It operates similarly to its 1-D counterpart in that it measures surface height from the same arbitrary point H below the board surface. Its

positioning is strategic in that pitch (z) is calculated about the center of the sensor span making it zero at the line scanner. This eliminates the need to remove pitch from 2-D height data contributing to further calculation efficiency. Roll (y) and translation (w) are the only rigid-body motions that need to be removed.

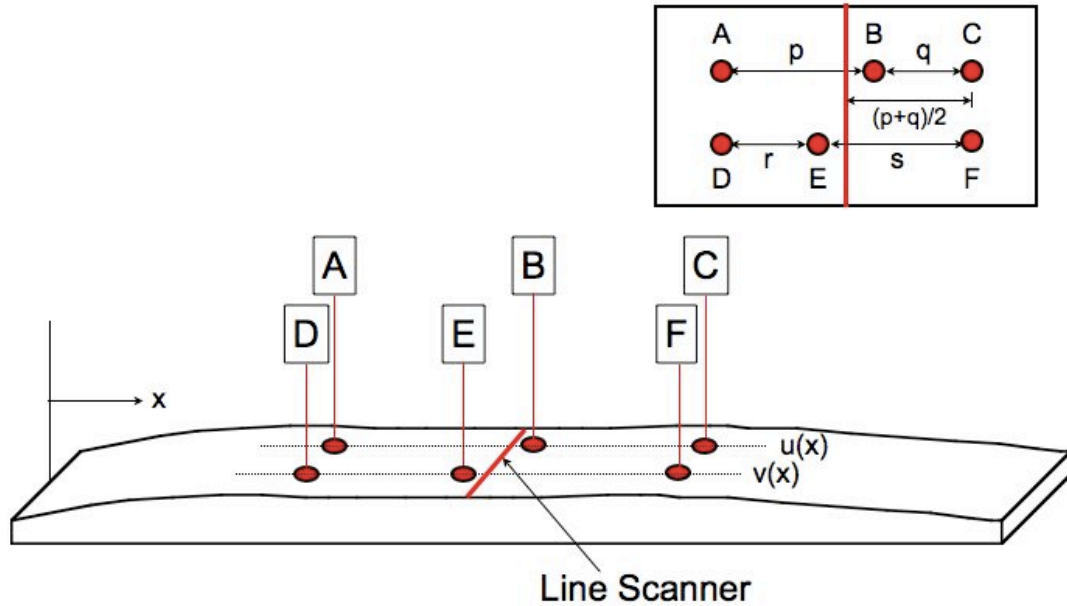


Figure 7: 2-D single-sided surface profiling arrangement

As mentioned earlier, surface measurement by the arrangement in Figure 4 begins when all sensors detect the board surface, and ends just before all sensors stop detecting the board surface. Adding a line scanner for 2-D data means that measurement must now commence when the line scanner detects the board surface and end just before it stops detecting the board surface in order to obtain 2-D data for the entire board. Because the line scanner is at mid-span, half of the point sensors will detect the surface when measurement begins and the other half will detect the surface when measurement ends. The rigid-body motion “profile” must now contain n points corresponding to every measurement taken by

the line scanner. Thus, each rigid-body motion can be eliminated from the entire 2-D data set and not just from the subset corresponding to when all point sensors detect the board surface.

Parallel-sided measurement with six sensors is broken up into five parts with the introduction of a line scanner at mid-span. The line scanner is activated in all measurement parts. Each part has a set of equations associated with it as shown in equations (19) through (23) below. For simplicity, $p=s$ and $q=r$. These parts are listed as follows:

1. The first part corresponds to when the line scanner is first activated and sensors B , C , and F are activated. Corresponding equations are shown below.

$$\begin{aligned}
 b_i - u_{i+(p-q)/2} &= w_i + y_i - \alpha \cdot z_i \\
 c_i - u_{i+(p-q)/2+q} &= w_i + y_i - z_i \quad 1 \leq i \leq (p-q)/2 \\
 f_i - v_{i+(p-q)/2+q} &= w_i - y_i - z_i
 \end{aligned} \tag{19}$$

where $\alpha=(p-q)/(p+q)$.

2. The second part corresponds to sensors B , C , F , and E being activated.

$$\begin{aligned}
 b_i - u_{i+(p-q)/2} &= w_i + y_i - \alpha \cdot z_i \\
 c_i - u_{i+(p-q)/2+q} &= w_i + y_i - z_i \\
 e_i - v_{i-(p-q)/2} &= w_i - y_i + \alpha \cdot z_i \\
 f_i - v_{i+(p-q)/2+q} &= w_i - y_i - z_i
 \end{aligned} \quad 1 + (p-q)/2 \leq i \leq (p-q)/2 + q \tag{20}$$

3. The third part contains measurements from all sensors A through F .

$$\begin{aligned}
 a_i - u_{i-(p-q)/2-q} &= w_i + y_i + z_i \\
 b_i - u_{i+(p-q)/2} &= w_i + y_i - \alpha \cdot z_i \\
 c_i - u_{i+(p-q)/2+q} &= w_i + y_i - z_i \\
 d_i - v_{i-(p-q)/2-q} &= w_i - y_i + z_i \\
 e_i - v_{i-(p-q)/2} &= w_i - y_i + \alpha \cdot z_i \\
 f_i - v_{i+(p-q)/2+q} &= w_i - y_i - z_i
 \end{aligned} \quad 1 + (p-q)/2 + q \leq i \leq (p-q)/2 + q + n_m \tag{21}$$

4. The fourth part corresponds to sensors A , B , D , and E being activated.

$$\begin{aligned}
a_i - u_{i-(p-q)/2-q} &= w_i + y_i + z_i \\
b_i - u_{i+(p-q)/2} &= w_i + y_i - \alpha \cdot z_i \\
d_i - v_{i-(p-q)/2-q} &= w_i - y_i + z_i \\
e_i - v_{i-(p-q)/2} &= w_i - y_i + \alpha \cdot z_i
\end{aligned}
\quad 1 + (p-q)/2 + q + n_m \leq i \leq n - (p-q)/2 \quad (22)$$

5. The fifth part corresponds to sensors A, D, and E being activated until the line scanner runs off the board.

$$\begin{aligned}
a_i - u_{i-(p-q)/2-q} &= w_i + y_i + z_i \\
d_i - v_{i-(p-q)/2-q} &= w_i - y_i + z_i \\
e_i - v_{i-(p-q)/2} &= w_i - y_i + \alpha \cdot z_i
\end{aligned}
\quad 1 + n - (p-q)/2 \leq i \leq n \quad (23)$$

$p-q$ is preferably an even number as the line scanner is positioned at $(p-q)/2$ at mid-span. Measurement index i goes from 1 to n as it corresponds to every measurement taken by the line scanner. Equations (21) are the same as equations (17) but are included here for completeness. Surface profiles u and v as well as sensor data are considered knowns in the above equations. This is because values of u and v from the reduced equations (16) are substituted into equations (19) through (23) to obtain the rigid-body motions corresponding to each line scanner measurement.

Least squares minimization is used to obtain three rigid-body motion equations for each measurement part as explained at the end of section 2.3.3. Fifteen equations in total are used to obtain all three rigid-body motions corresponding to each line scanner measurement. Since pitch (z) need not be removed from the 2-D data, a total of $2(n)$ forward calculations are performed to obtain roll (y) and translation (w). Due to the measures taken to enhance calculation economy, the time necessary to perform the inverse calculation and determine all rigid-body motions is approximately 1/4 of the time taken in Gazzarri's [16] method.

2.4 Removal of Rigid-Body Motions

There are n values of translation (w) and roll (y) corresponding to n measurements taken by the 2-D line scanner. Each rigid-body motion must be eliminated from the raw 2-D data. Before removal, however, the mean of each rigid-body motion data set must be subtracted from the set. This is due to how the boundary conditions of the system are defined. The first values of u and v are set to zero indicating that the beginning of the board starts at zero height. Each successive height is, thus, relative to zero. Actual board height is then considered a rigid-body translation and is transferred to w . By removing the mean from w , this “left-over” board height is removed. Pure translation remains.

Setting the first values of both u and v to zero also indicates that there is no twist at the beginning of the board. Therefore, any actual twist present is considered rigid-body roll and transferred to y . Removing the mean from y is essentially removing this “left-over” twist. Pure roll remains.

Removing translation from 2-D data is straightforward. Because translation is simply the rigid elevation of the board, each value of w is the same at every sensor. Thus, each value of w can be subtracted from its corresponding 2-D measurement.

Removing roll information from the 2-D data is trickier. The height of the board due to roll recorded by sensors A , B , and C is $+y$, while that recorded by sensors D , E , and F is $-y$. This is evident in equations (5) and illustrated in Figure 8. The lines formed by sensors ABC and DEF (u -line and v -line, respectively) must be identified in the 2-D scanner data. The 2-D scanner is comprised of many rays. Thus, the single ray closest to each line is assigned to that line. This eliminates the necessity that the line scanner be positioned symmetrically among point scanners. Note that the rays pictured in Figure 8 are drawn

vertically for simplicity but are actually emitted from the 2-D scanner at an angle. This does not affect ray assignment to each line because a ray is assigned to each line for every measurement. Therefore, a shift in board that would cause u and v -lines to align with different rays during scan does not affect accuracy of roll subtraction.

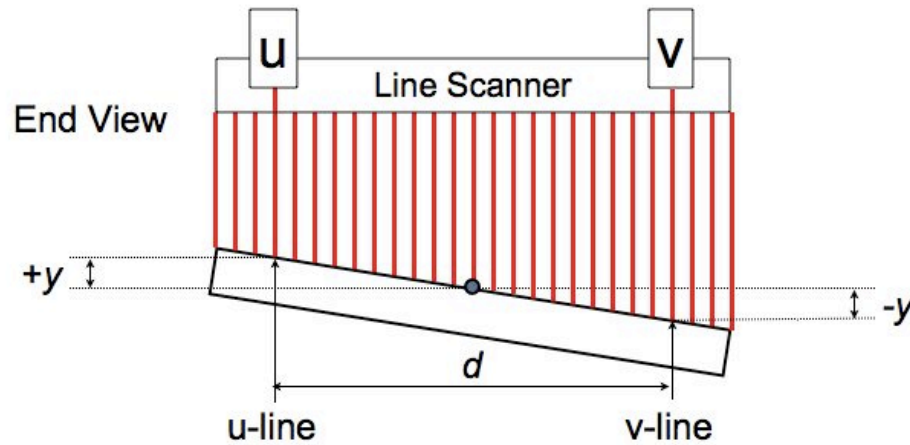


Figure 8: Identifying u-line and v-line in line scanner

Once two rays corresponding to the u and v -lines have been identified, the slope of the board at each 2-D measurement (i) is calculated according to (24).

$$slope = \frac{2 \cdot y_i}{d} \quad 1 \leq i \leq n \quad (24)$$

where d is the distance between u -line and v -line. Once the slope has been calculated, y_i can be interpolated across all remaining rays of the line scanner based on the known distance between each ray. Once the height due to roll is known at each ray, it is subtracted accordingly. What is left is an accurate depiction of the 2-D board surface.

2.5 Parallel Profiling with 8 Point Sensors

Parallel profiling using six sensors requires a board that is at least three times the sensor span ($p+q$) in length in order to have enough data to produce a solution according to

equations (7). Given that a line scanner is now present at mid-span, this widens the gap between middle sensors B and E . In order to maintain accurate identification of curvature in a board, the spacing between middle sensors must be relatively small compared to outer sensors. Thus, the presence of a line scanner results in an overall wider sensor span. The wider the span, the longer the scanned board needs to be. This can be inconvenient when needing to measure shorter boards. The addition of two point sensors in the parallel-sided profiling arrangement alleviates this inconvenience by introducing more data.

Additional data also allows more data averaging to occur, reducing noise. This is helpful because the minimum boundary of the line laser field of view is typically further than that for point lasers. However, point lasers lose accuracy at further distances causing noisier data. Two extra point sensors result in smoother data contributing to a more accurate rigid-body motion solution. The eight-sensor parallel profiling arrangement is shown in Figure 9.

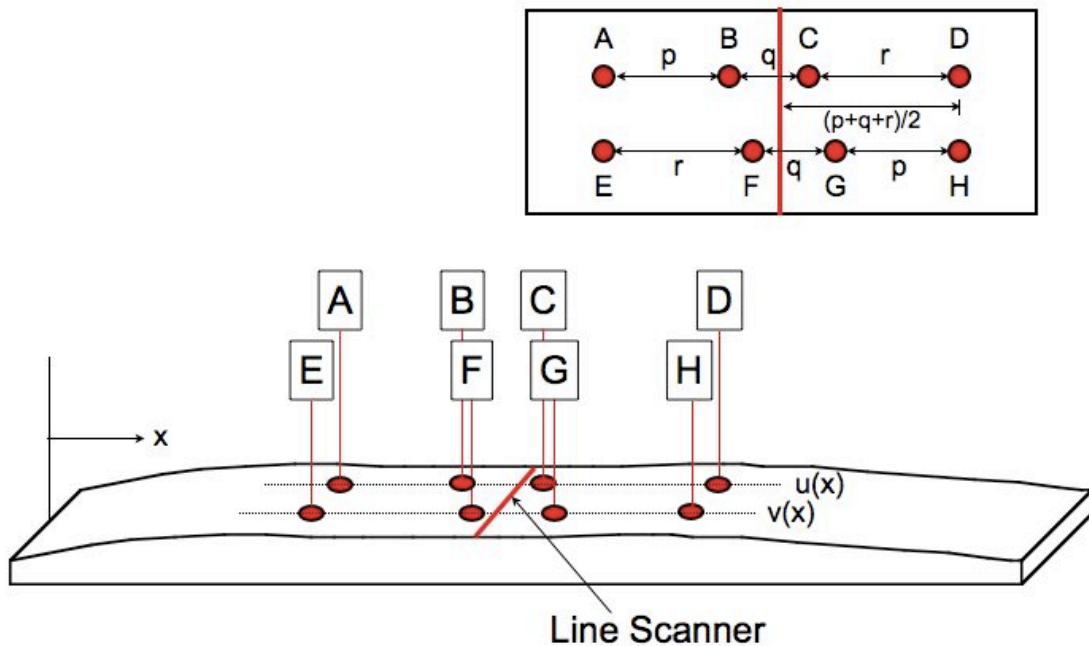


Figure 9: 2-D surface profiling with eight sensors

The former six-sensor arrangement comprises sensors A , C , D , E , F , and H . The addition of sensors B and G add two equations to (5) as seen in equations (25) below. Sensors B and G are offset from sensors F and C to reduce the effect of nulls caused by sensor spacings with common or very similar multiples. Varying the spacing between sensors reduces the possibility that a null is touched. Sensors B and G are also placed symmetrically within the six-sensor arrangement as to avoid any difference in accuracy between either ends of u and v . This creates three sensor spacings p , q , and r where $r > p > q$.

$$\begin{aligned}
(1) \ a_i &= u_i + w_i + y_i + z_i \\
(2) \ b_i &= u_{i+p} + w_i + y_i + \gamma \cdot z_i \\
(3) \ c_i &= u_{i+p+q} + w_i + y_i - \alpha \cdot z_i \\
(4) \ d_i &= u_{i+p+q+r} + w_i + y_i - z_i \\
(5) \ e_i &= v_i + w_i - y_i + z_i \\
(6) \ f_i &= v_{i+r} + w_i - y_i + \alpha \cdot z_i \\
(7) \ g_i &= v_{i+r+q} + w_i - y_i - \gamma \cdot z_i \\
(8) \ h_i &= v_{i+r+q+p} + w_i - y_i - z_i
\end{aligned} \quad 1 \leq i \leq n_m \quad (25)$$

where $\gamma = (-p+q+r)/(p+q+r)$ and $\alpha = (p-q+r)/(p+q+r)$ and are the fractional heights of pitch for inner sensors. n_m is the number of measurements taken while all points are activated by the board surface and equals $n-p-q-r$. Reducing equations (25) is done similarly as for the six-sensor arrangement. The equations are combined and manipulated to eliminate y , w and z in that order. Five equations in terms of u and v remain. The order of combination is illustrated in Figure 10 and shown symbolically in Equations (26) through (28).

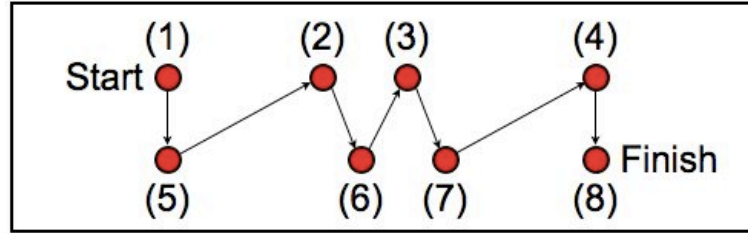


Figure 10: Order of equation combination for bandwidth minimization using eight sensors

$$\begin{aligned}
 (9) &= (1) + (5) \\
 (10) &= (5) + (2) \\
 (11) &= (2) + (6) \\
 (12) &= (6) + (3) \\
 (13) &= (3) + (7) \\
 (14) &= (7) + (4) \\
 (15) &= (4) + (8)
 \end{aligned} \tag{26}$$

$$\begin{aligned}
 (16) &= (9) - (10) \\
 (17) &= (10) - (11) \\
 (18) &= (11) - (12) \\
 (19) &= (12) - (13) \\
 (20) &= (13) - (14) \\
 (21) &= (14) - (15)
 \end{aligned} \tag{27}$$

$$\begin{aligned}
 (22) &= (1 - \alpha)(16) - (1 - \gamma)(17) \\
 (23) &= (\alpha + \gamma)(17) - (1 - \alpha)(18) \\
 (24) &= (18) - (19) \\
 (25) &= (1 - \alpha)(19) - (\alpha + \gamma)(20) \\
 (26) &= (1 - \gamma)(20) - (1 - \alpha)(21)
 \end{aligned} \tag{28}$$

Equations (28) are written out in equations (29) below.

$$\begin{aligned}
(1-\alpha)[A_i - B_i] - (1-\gamma)[E_i - F_i] &= (1-\alpha)u_i & - (1-\alpha)u_{i+p} & - (1-\gamma)v_i & + (1-\gamma)v_{i+r} \\
(\alpha+\gamma)[E_i - F_i] - (1-\alpha)[B_i - C_i] &= (\alpha+\gamma)v_i & - (\alpha+\gamma)v_{i+r} & - (1-\alpha)u_{i+p} & + (1-\alpha)u_{i+p+q} \\
B_i - C_i - F_i + G_i &= u_{i+p} & - u_{i+p+q} & - v_{i+r} & + v_{i+r+q} \\
(1-\alpha)[F_i - G_i] - (\alpha+\gamma)[C_i - D_i] &= (1-\alpha)v_{i+r} & - (1-\alpha)v_{i+r+q} & - (\alpha+\gamma)u_{i+p+q} & + (\alpha+\gamma)u_{i+p+q+r} \\
(1-\gamma)[C_i - D_i] - (1-\alpha)[G_i - H_i] &= (1-\gamma)u_{i+p+q} & - (1-\gamma)u_{i+p+q+r} & - (1-\alpha)v_{i+r+q} & + (1-\alpha)v_{i+r+q+p}
\end{aligned} \tag{29}$$

$$1 \leq i \leq n_m$$

Equations (29) are solved for u and v using least squares minimization. Once u and v are obtained, they are substituted into equations (30) through (36) to determine the full end-to-end rigid-body motion “profile” for translation and roll. Due to the additional two sensors and their skew arrangement within the former six-sensor setup, there are now seven parts of end-to-end 2-D scanning for which a different set of point sensors are activated. Each rigid-body motion solution from each part combines to form the full rigid-body motion “profile.”

$$\begin{aligned}
c_i - u_{i+j/2} &= w_i + y_i - \alpha \cdot z_i \\
d_i - u_{i+j/2+r} &= w_i + y_i - z_i \\
g_i - v_{i+k/2} &= w_i - y_i - \gamma \cdot z_i \\
h_i - v_{i+k/2+p} &= w_i - y_i - z_i
\end{aligned} \quad 1 \leq i \leq j/2 \tag{30}$$

$$\begin{aligned}
c_i - u_{i+j/2} &= w_i + y_i - \alpha \cdot z_i \\
d_i - u_{i+j/2+r} &= w_i + y_i - z_i \\
f_i - v_{i-j/2} &= w_i - y_i + \alpha \cdot z_i \\
g_i - v_{i+k/2} &= w_i - y_i - \gamma \cdot z_i \\
h_i - v_{i+k/2+p} &= w_i - y_i - z_i
\end{aligned} \quad 1 + j/2 \leq i \leq k/2 \tag{31}$$

$$\begin{aligned}
b_i - u_{i-k/2} &= w_i + y_i + \gamma \cdot z_i \\
c_i - u_{i+j/2} &= w_i + y_i - \alpha \cdot z_i \\
d_i - u_{i+j/2+r} &= w_i + y_i - z_i \\
f_i - v_{i-j/2} &= w_i - y_i + \alpha \cdot z_i \\
g_i - v_{i+k/2} &= w_i - y_i - \gamma \cdot z_i \\
h_i - v_{i+k/2+p} &= w_i - y_i - z_i
\end{aligned} \quad 1 + k/2 \leq i \leq k/2 + p \tag{32}$$

$$\begin{aligned}
a_i - u_{i-k/2-p} &= w_i + y_i + z_i \\
b_i - u_{i-k/2} &= w_i + y_i + \gamma \cdot z_i \\
c_i - u_{i+j/2} &= w_i + y_i - \alpha \cdot z_i \\
d_i - u_{i+j/2+r} &= w_i + y_i - z_i \\
e_i - v_{i-j/2-r} &= w_i - y_i + z_i \\
f_i - v_{i-j/2} &= w_i - y_i + \alpha \cdot z_i \\
g_i - v_{i+k/2} &= w_i - y_i - \gamma \cdot z_i \\
h_i - v_{i+k/2+p} &= w_i - y_i - z_i
\end{aligned} \quad 1+k/2+p \leq i \leq k/2+p+nm \quad (33)$$

$$\begin{aligned}
a_i - u_{i-k/2-p} &= w_i + y_i + z_i \\
b_i - u_{i-k/2} &= w_i + y_i + \gamma \cdot z_i \\
c_i - u_{i+j/2} &= w_i + y_i - \alpha \cdot z_i \\
e_i - v_{i-j/2-r} &= w_i - y_i + z_i \\
f_i - v_{i-j/2} &= w_i - y_i + \alpha \cdot z_i \\
g_i - v_{i+k/2} &= w_i - y_i - \gamma \cdot z_i
\end{aligned} \quad 1+k/2+p+nm \leq i \leq n-k/2 \quad (34)$$

$$\begin{aligned}
a_i - u_{i-k/2-p} &= w_i + y_i + z_i \\
b_i - u_{i-k/2} &= w_i + y_i + \gamma \cdot z_i \\
c_i - u_{i+j/2} &= w_i + y_i - \alpha \cdot z_i \\
e_i - v_{i-j/2-r} &= w_i - y_i + z_i \\
f_i - v_{i-j/2} &= w_i - y_i + \alpha \cdot z_i
\end{aligned} \quad 1+n-k/2 \leq i \leq n-j/2 \quad (35)$$

$$\begin{aligned}
a_i - u_{i-k/2-p} &= w_i + y_i + z_i \\
b_i - u_{i-k/2} &= w_i + y_i + \gamma \cdot z_i \\
e_i - v_{i-j/2-r} &= w_i - y_i + z_i \\
f_i - v_{i-j/2} &= w_i - y_i + \alpha \cdot z_i
\end{aligned} \quad 1+n-j/2 \leq i \leq n \quad (36)$$

where j is the horizontal distance ($p+q-r$) between sensors C and F and k is the distance ($q+r-p$) between sensors B and G . These two values are preferably even as the line laser is positioned at both $j/2$ and $k/2$ at mid-span.

Least squares minimization is again used to determine three equations corresponding to w , y and z for each part of the 2-D scan (21 equations total). Pitch (z) does not need to be removed from the 2-D data. Therefore, 14 equations (7 for translation and 7 for roll) are

directly entered into the computer program accompanying this setup. Values of u and v and data from each point sensor are substituted into these 14 equations making it a simple forward calculation to determine translation and roll. These two rigid-body motions can then be removed from the 2-D data using the same method as discussed in section 2.4. An accurate 2-D surface height profile remains.

2.6 Double-Sided 2-D Surface Profiling

One of the objectives of this work was to be able to obtain separate-sided 2-D surface profiles, or profiles of a surface completely independent of the opposite surface. Measuring a single surface of the board and removing rigid-body motions from this data ensures that the profile is indeed independent of the opposite side. A double-sided profile can then be determined using this same methodology. This enhances process control of a sawmill because typically a different machine or saw cuts each side of the board. Therefore, knowing the location of a surface defect on the board will point to the location of a problem in the milling process.

Double-sided profiling is conceptually straightforward. A second line laser is placed directly below the top line laser so that their rays are offset by 3mm. This prevents saturation of each line scanner's CCD camera but is still close enough to assume the two are aligned. The second line scanner is synchronized with every sensor in the setup. Similar to the top line laser, it begins 2-D measurement once it detects the board surface collecting 2-D information along the underside of the board. Again the data are inverted so as to measure the surface from a point H arbitrarily positioned above the underside of the board. Because the

board cannot fall below the conveyor, H is set at the top of the conveyor rollers. Figure 11 illustrates this configuration.

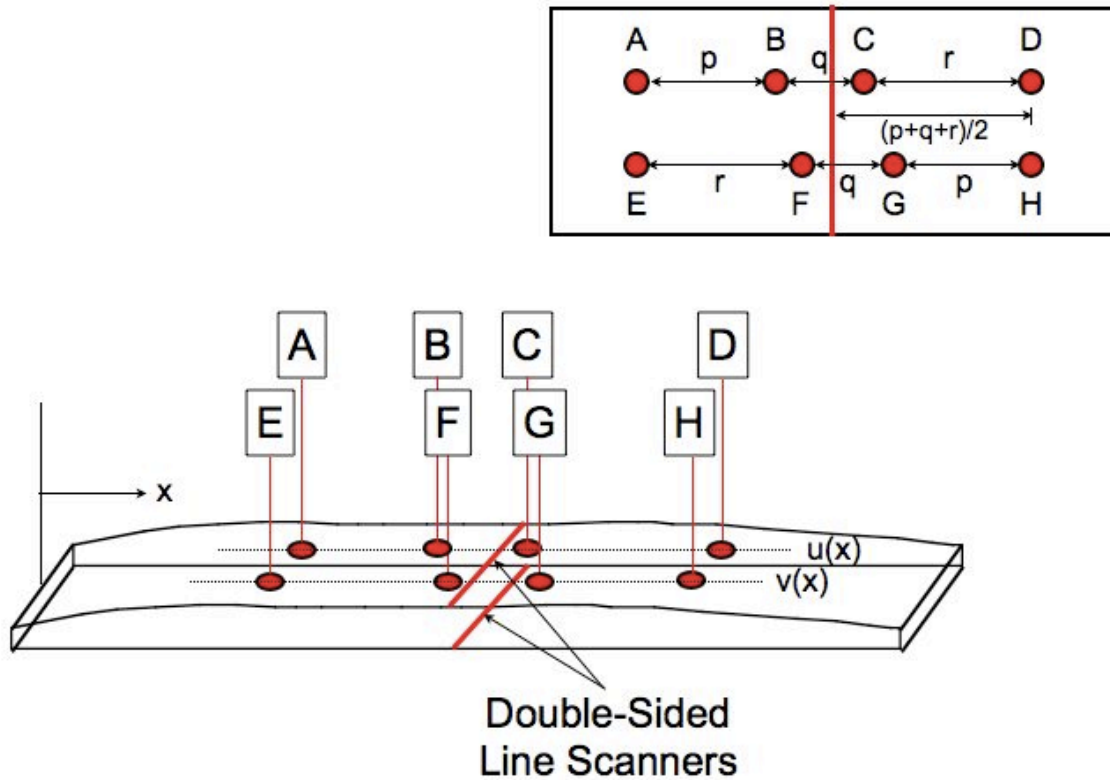


Figure 11: Double-sided 2-D surface profiling arrangement

At the end of measurement, each rigid-body motion profile is removed from the bottom 2-D data using the same method described in section 2.4. However, instead of subtracting each rigid-body motion value from the 2-D data, it is added. An accurate 2-D surface profile remains for the bottom surface of the board.

Thickness information over the entire board can also be determined with double-sided line scanners. Each ray of *Line Scanner 1* is aligned with a ray in *Line Scanner 2* based on its position along the y -axis. This is shown in Figure 12 below, where L_1 and L_2 are the raw range readings from each scanner to the board surface. The 2-D thickness profile can be found using equation (37).

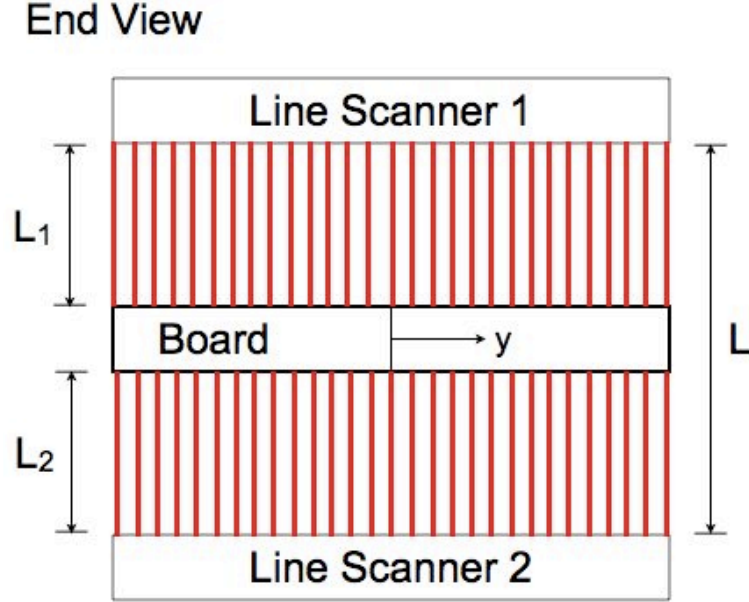


Figure 12: Thickness measurement using double-sided 2-D line scanners

$$\begin{aligned}
 \text{Thickness} &= L_{ij} - L_{1ij} - L_{2ij} \\
 1 \leq j &\leq \text{raynum}_{\max} \\
 1 \leq i &\leq n
 \end{aligned} \tag{37}$$

where i is the ray index and j is the measurement index.

2.7 Regularization and Smoothing

Inverse problems are typically ill-conditioned for two reasons. One, columns in the kernel matrix G may not be linearly independent. Thus, the $G^T G$ matrix cannot be inverted. Two, the ratio of largest to smallest eigenvalues known as the *condition number* of $G^T G$ may be very large causing instability in the inverse solution. The result is noise present in the data becomes amplified in the solution. The condition number worsens for large n making it problematic to identify the solution properly in the case of surface profiling. Tikhonov regularization is commonly used to smooth an inverse solution and improve its accuracy [21, 22, 23]

Regularization parameter β is chosen according to Morozov's Discrepancy Principle stating that the data misfit $\|G \cdot m - d^{obs}\|$ should equal the data noise level. This is because further improvement of the data fit beyond the average error in the data is not useful [22]. Under the assumption that the standard deviations of all misfit errors are the same $\sigma_i = \sigma$, β is set in order to satisfy equation (42). Equations (38) and (42) are solved iteratively until a value for β converges.

$$\left[\frac{G \cdot m - d^{obs}}{\sigma} \right]^2 = N \quad (42)$$

where N is the total number of data points.

Regularization is added to $G^T G$ in equation (38) smoothing 1-D profiles u and v . However, after u and v are substituted into rigid-body motion equations (30) through (36), noise in the sensor data is still amplified in the rigid-body motion solution. Smoothing u and v increases accuracy in the solution, but it is still difficult to identify it amongst amplified noise. Therefore, further smoothing is applied to each rigid-body motion "profile" before removing it from the 2-D data.

Binomial smoothing, also known as binomial or Gaussian filtering [24], is used to remove high frequency variation in the rigid-body motion solutions. It is a common filtering technique that involves convolving a set of $(2N_p + 1)$ coefficients with a data array, where N_p is any integer. In this work, $N_p = 1$ yielding a three-point binomial filter. The coefficient set b_k can be found using the following equation.

$$b_k = \binom{2N_p}{N_p + k} / 4^{N_p} \quad (k = 0, 1, \dots, N_p) \quad (43)$$

where $b_{-k} = b_k$. Setting $N_p = 1$ yields $b_{-1,0,1} = \{1/4, 1/2, 1/4\}$. This particular filter is called three-

point because it essentially passes a least squares parabola through three data points. Deviations from this parabola are considered noise and are then smoothed [25]. In order to associate each point with more than just its adjacent points, the three-point filter is passed through the data set multiple times until desired smoothness is obtained. Similar to Tikhonov regularization, a balance exists in attenuating noise while maintaining true features of the solution.

Chapter 3: Experiment and Results

3.1 Experimental Set-Up

This chapter presents practical demonstrations of the method described in Chapter 2. The experimental set-up shown in Figures 13 and 14 was used to conduct all 2-D surface profiling tests. The sensors are arranged in the 8-sensor, double-sided profiling configuration shown in Figure 11 with physical spacings of $p=198\text{mm}$, $q=111\text{mm}$ and $r=213\text{mm}$. Measurement step size was 3mm for all tests.

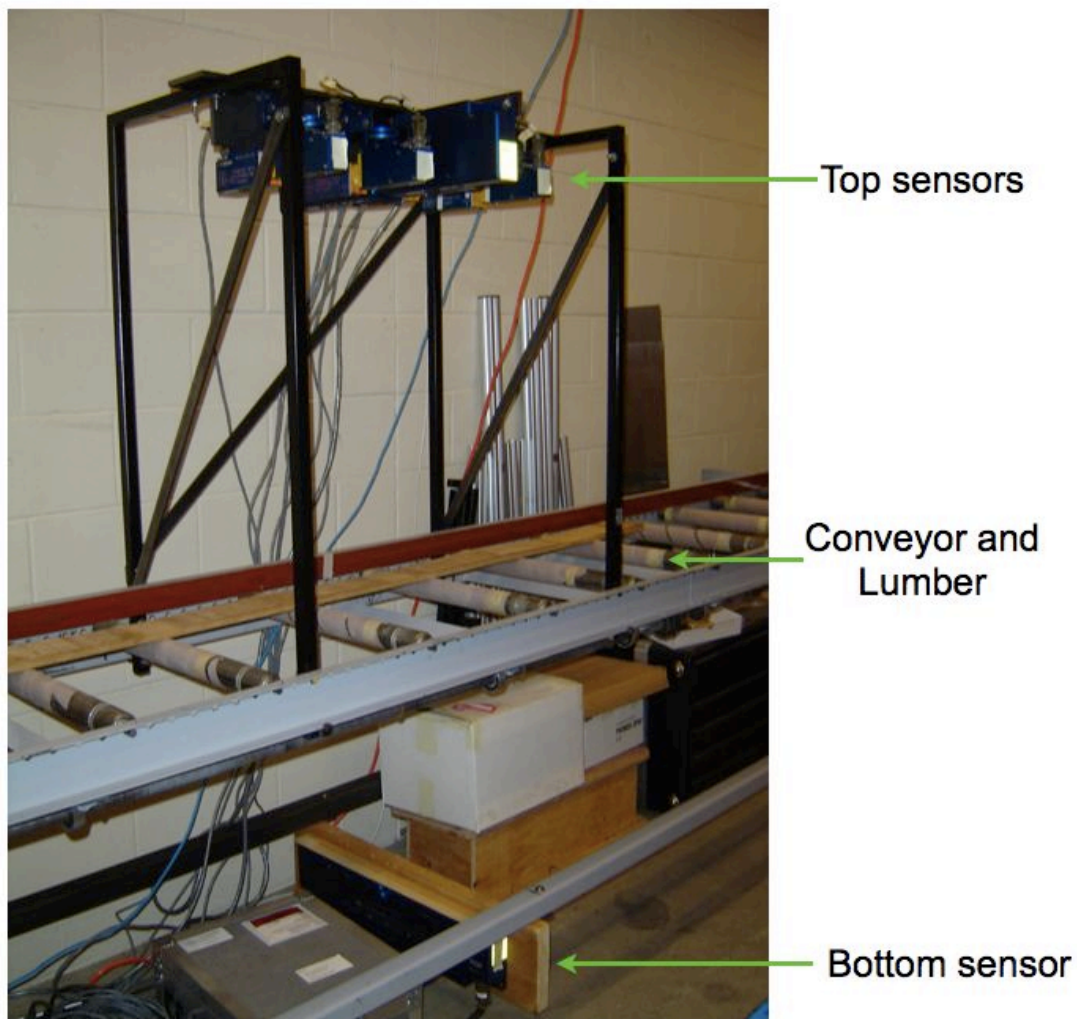
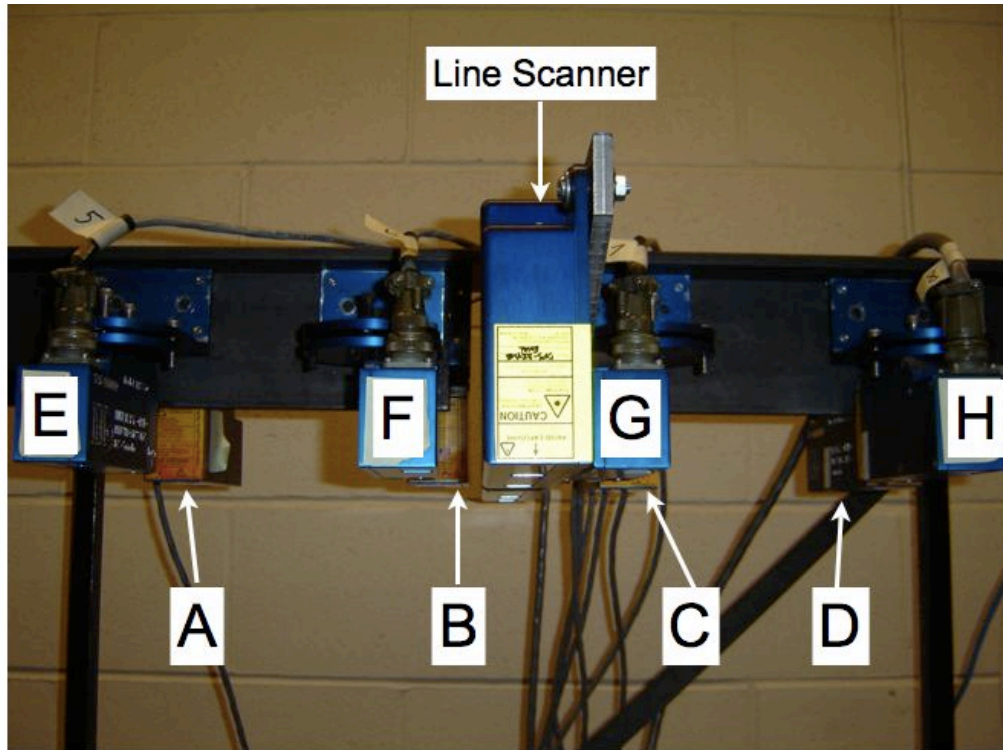


Figure 13: Experimental set-up; 8 point sensors and 2 line sensors



**Figure 14: Close-up front view of all top sensors
Sensors ABCD behind EFGH**

The set-up included a total of ten triangulation lasers manufactured by Hermery Opto Electronics Inc. Eight of the ten lasers were laser range sensors (LRS-50) that provided 1-D measurements. They have an active range of 125-1650mm. Resolution at 125mm is 0.05mm and exponentially worsens with distance from the measured surface. The LRS 16 Head Concentrator (LRS-16HC) also manufactured by Hermery Opto Electronics Inc. performed signal conditioning of LRS data.

The other two triangulation sensors in the set-up were Dual Profile Board Scanners (DPS-824) capable of 2-D geometric surface measurements. Geometric data were recorded by a series of 63 rays that are spaced approximately 6mm apart. Each ray recorded 1-D data along the length of a board. Interpolation between adjacent rays provided 2-D information for the entire board surface. The active range of DPS-824 is 508-812mm with a resolution of

0.1mm at close range. A head concentrator also manufactured by Hermary Opto Electronics Inc. and able to accommodate two DPS heads performed signal processing on DPS data. Both LRS and DPS head concentrators are capable of 1kHz sample rate.

All laser sensors were initially calibrated before measurement and subsequently calibrated after any alteration of the laser position. Calibration involved scanning a flat board with known height, width slightly less than that of each conveyor roller, and length longer than sensor span. Having a width slightly less than that of each roller ensured that the majority of line scanner rays would be activated. Having a length longer than the sensor span provided multiple measurements from each sensor that could be averaged. This reduced errors caused by noise. Board height was added to each average sensor reading creating an offset for each sensor. Each offset was removed from all subsequent sensor readings providing a measurement of surface height starting from the top conveyor surface for top sensors. The known height of the calibration board above the top conveyor surface marked the point from which lower side profiles were measured by the bottom sensor. This was done for point and line scanners alike. Calibration ensured that not all sensors had to be perfectly aligned in the vertical direction and that each line scanner need not be exactly parallel to the conveyor surface.

The laser sensors were mounted approximately 680mm above and below an industrial style conveyor capable of transportation speeds equivalent to those in a sawmill. All rollers were spaced 310mm apart and are approximately 160mm in circumference. Each roller of the conveyor was lined with sandpaper as to prevent slippage between roller and lumber. A BEI® E25 incremental optical encoder with resolution of 2500 pulses per revolution tracked

linear position of the board during scanning. It measured the angular position of the shaft responsible for rotating all conveyor rollers.

Each head concentrator was equipped with an encoder port, allowing all laser sensor data (1-D and 2-D) to be synchronized on the same encoder count. Synchronizing based on encoder counts rather than time eliminated the need to know and/or control conveyor speed. Thus, all measurements were recorded based on linear displacement of the scanned board.

All sensor data was reported to a personal computer from the head concentrators via Ethernet connection. Forintek and UBC jointly developed drivers for both LRS and DPS lasers. Both drivers were written in C (programming language). They organized all sensor data for use by the surface profiling algorithm written in FORTRAN.

3.2 Six Sensors Versus Eight Sensors

The advantage of employing two additional sensors in the original six sensor parallel-sided profiling arrangement was first investigated. Each set's performance in accurately recovering 1-D parallel profiles of the top surface of a custom-cut board was evaluated and compared. The accuracy of 1-D profiles u and v directly affects the accuracy of rigid-body motion profiles and, thus, the accuracy of 2-D profiles, as rigid-body motion information is removed from 2-D data. All 8 sensors with spacings p , q and r took sequential height measurements of a board with one sinusoidal-cut surface (top) and one flat surface (bottom). Both surfaces were smooth to the touch. A 80mm square smooth plate with thickness of 6mm was placed on the top surface at approximately 600mm from the beginning of the board. The step was wide enough to be detected by both lines of sensors during measurement. Six-sensor data was chosen out of the 8-sensor data, as 6-sensor spacings were simply a combination of

8-sensor spacings p , q and r . Therefore, the same raw data set was used in the following demonstrations of 6-sensor and 8-sensor performance. Six-sensor spacings were $p=309\text{mm}$, $q=213\text{mm}$, $r=q$, and $s=p$.

Figures 15 and 16 show the recovered 1-D parallel profiles as calculated by each sensor arrangement. No regularization was applied as to show the true noise amplification in each solution. Noise amplification is the ratio of noise content in the recovered solution to noise content in the raw data.

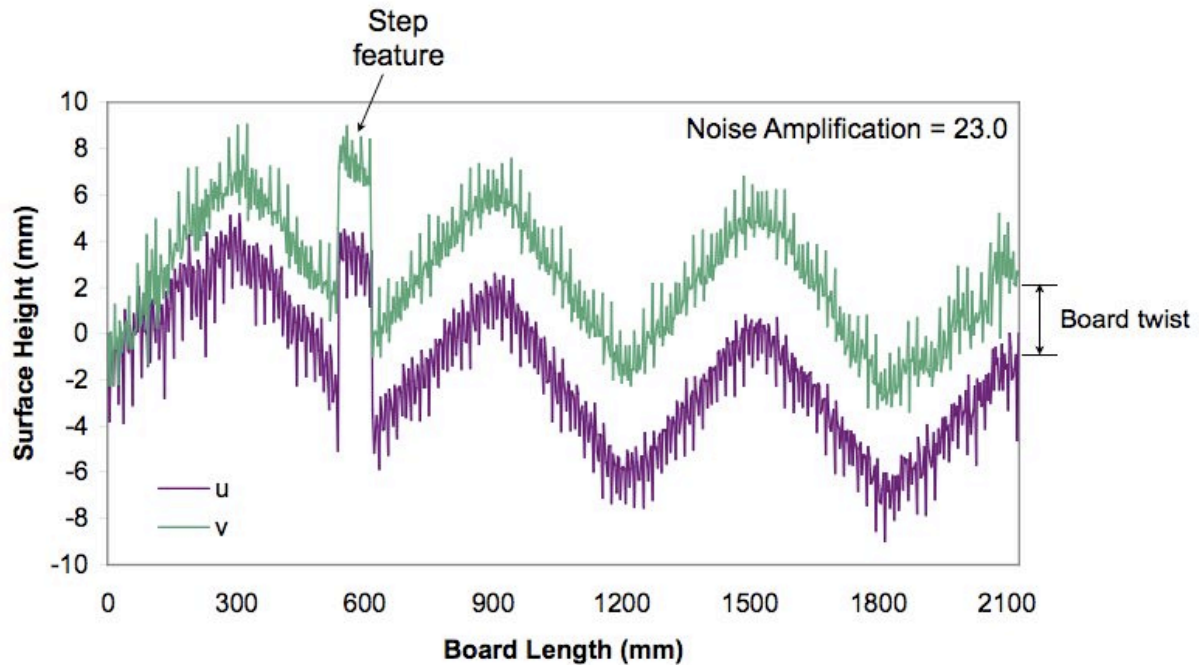


Figure 15: 6 Sensor 1-D parallel profiles of top surface of sinusoidal board – no regularization

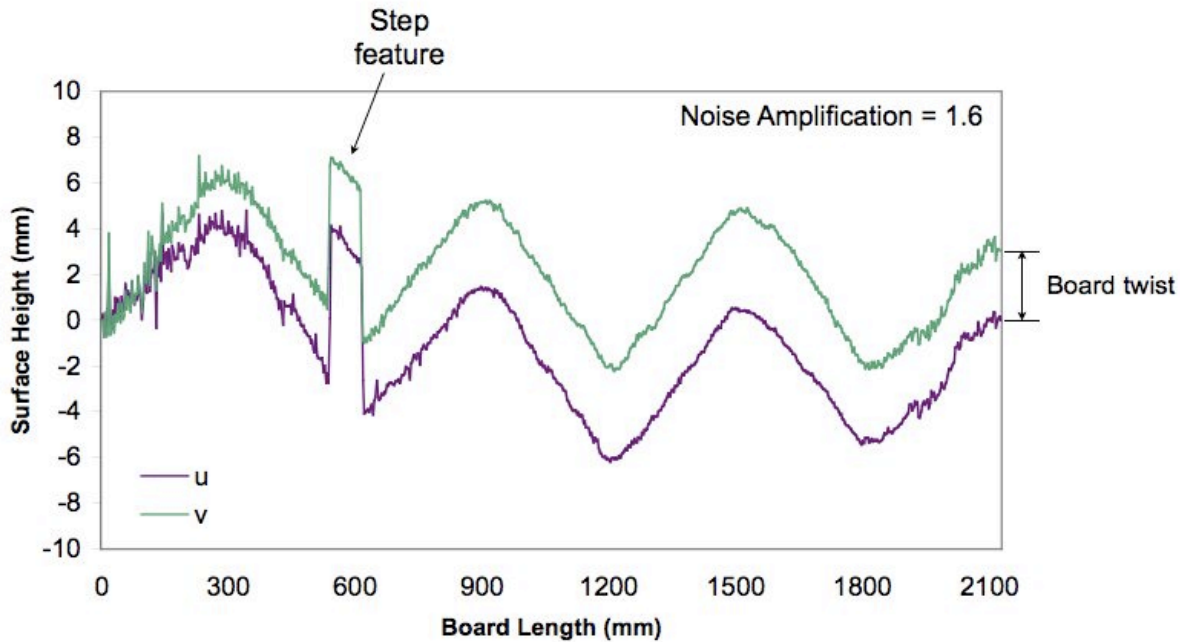


Figure 16: 8 Sensor 1-D parallel profiles of top surface of sinusoidal board – no regularization

Less data averaging occurs for 6 sensors resulting in a noisier solution and a noise amplification that is 14 times greater than that of 8 sensors. As a result, a higher level of regularization must be applied to remove high frequency content from the solution. Regularization however, is essentially a form of distortion. Although high levels of regularization remove high frequency noise, they do not necessarily equate to higher accuracy.

The same amount of regularization was applied to both 6-sensor and 8-sensor solutions as seen in Figures 17 and 18 below. While both solutions are smoother, more definition of the step feature is retained in the 8-sensor solution. The difference is small. However, the ability to resolve detail becomes more important for boards with rough surfaces. This is because surface roughness is typically on the order of less than a millimeter.

In order to maintain a high level of accuracy (less than 0.5mm) in the 2-D profile, these surface features must be retained without being smoothed by regularization.

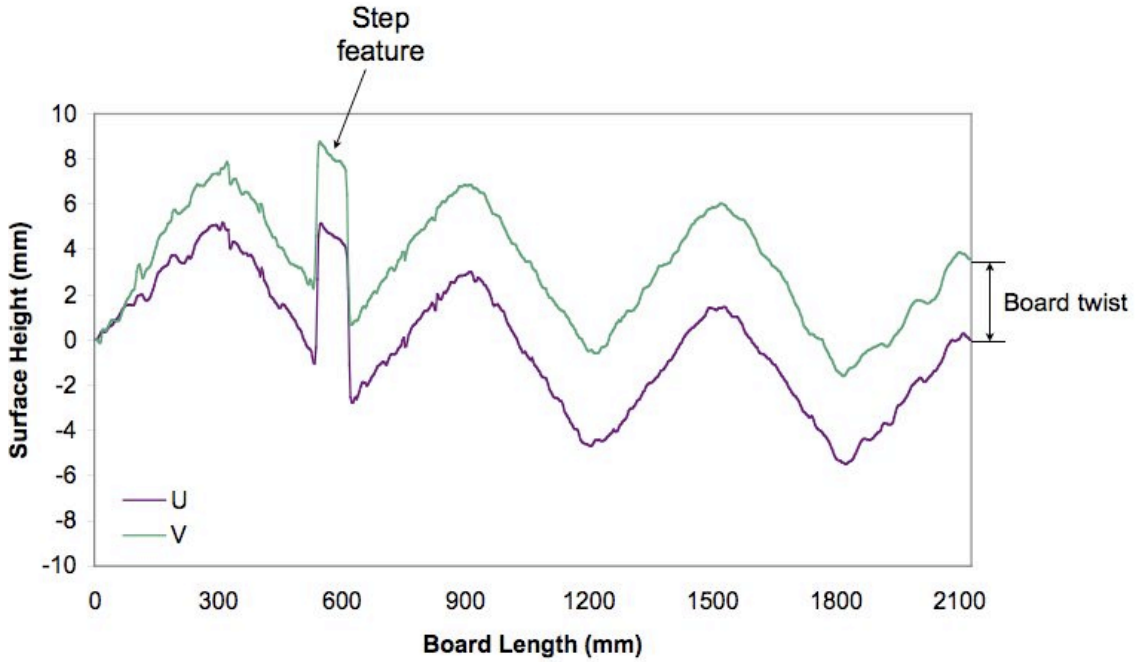


Figure 17: 6 Sensor parallel 1-D profiles of top surface of sinusoidal board – with regularization: $\alpha_{flat}=0.1, \alpha_{smooth}=1.0$

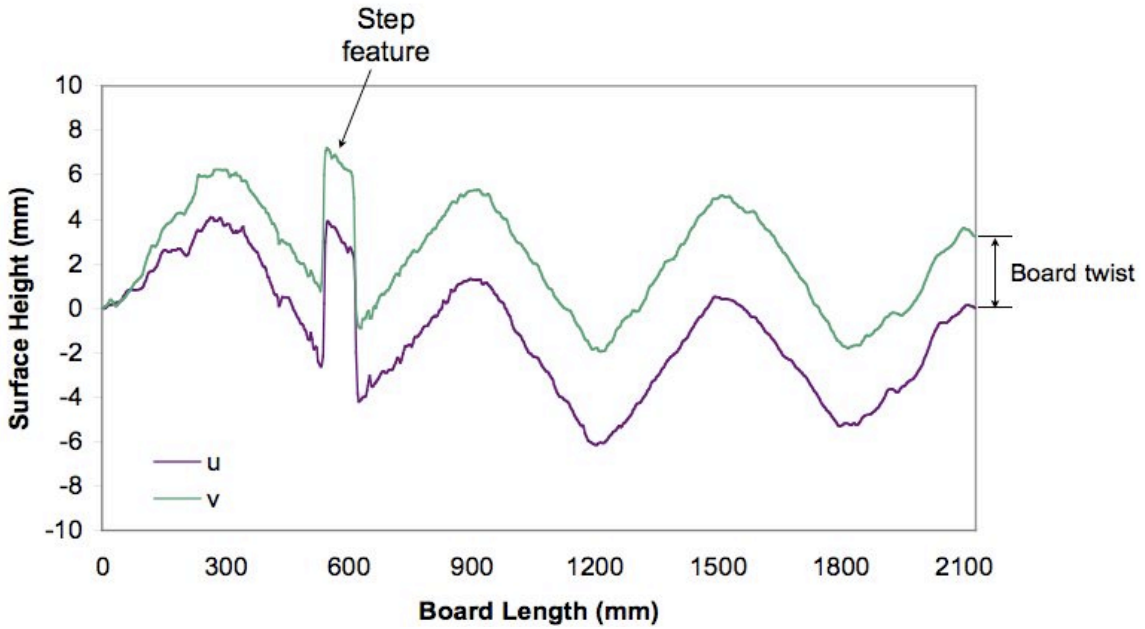


Figure 18: 8 Sensor parallel 1-D profiles of top surface of sinusoidal board – with regularization: $\alpha_{flat}=0.1, \alpha_{smooth}=1.0$

3.3 Removal of Rigid-Body Motions

Two cases are presented demonstrating the 2-D profiling system's ability to remove rigid-body motion content from raw 2-D surface height data. The first case involves the measurement of a flat board with a known rigid-body motion introduced into the system. The board's dimensions were 1750mmx250mm. A step with dimensions 178mmx6mmx1.3mm was positioned as shown in Figure 19 on each of four conveyor rollers directly below the laser sensor arrangement. All steps were aligned as to come into contact with the traversing board simultaneously, creating a mostly translational rigid-body motion. Translation occurred with every rotation of the rollers. This is a severe test, as rigid-body motions are typically subtler in an actual sawmill.

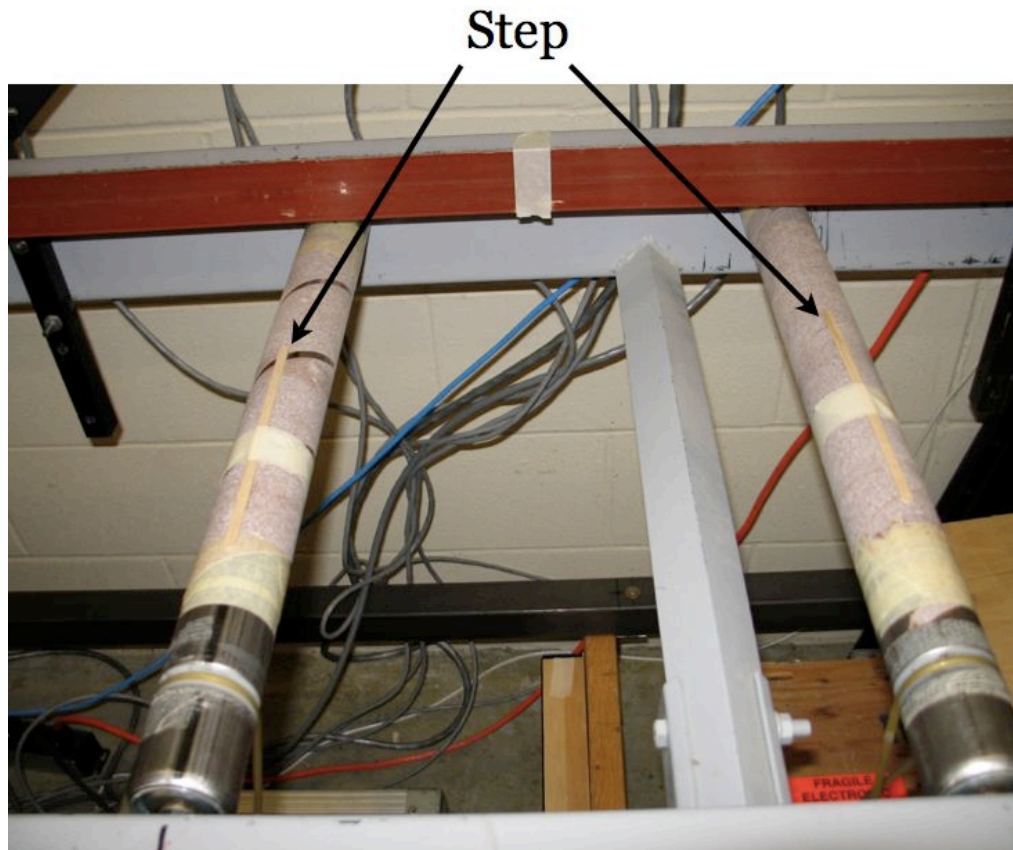


Figure 19: Step placed on center 4 rollers to introduce known translation

The 8-sensor 2-D scanning arrangement with spacings listed in the previous section was used for this demonstration and all following demonstrations. Single-sided measurements only are presented as to showcase particular features on one side of each test board. The 2-D raw data for the top surface is presented in Figure 20. Note that the legend at the right is in millimeters. The translation effects due to the roller step are indicated in the 2-D data by the repetitive change in color evenly spaced by the circumference of the rollers. A fainter change in color adjacent to each translation spike is also present. This is a separate rigid translation of the board due to a slight eccentricity of each roller.

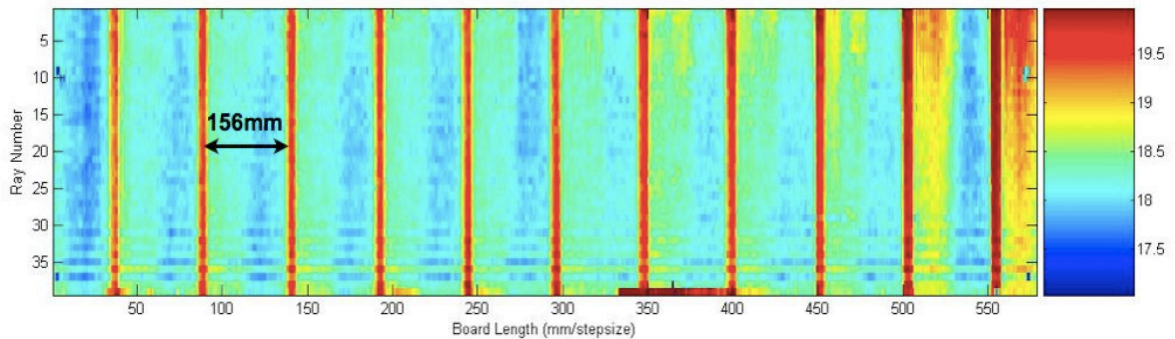


Figure 20: Raw 2-D data for flat board with translational rigid-body motion

One-dimensional data from all eight 1-D scanners are presented in Figure 21. Repetitive translation due to the step and eccentric rollers appears at all sensors. Figure 22 shows the end-to-end translation profile calculated from the raw 1-D data using the parallel-sided profiling algorithm. The distance between translation peaks corresponds to the distance between those seen in the raw 2-D data.

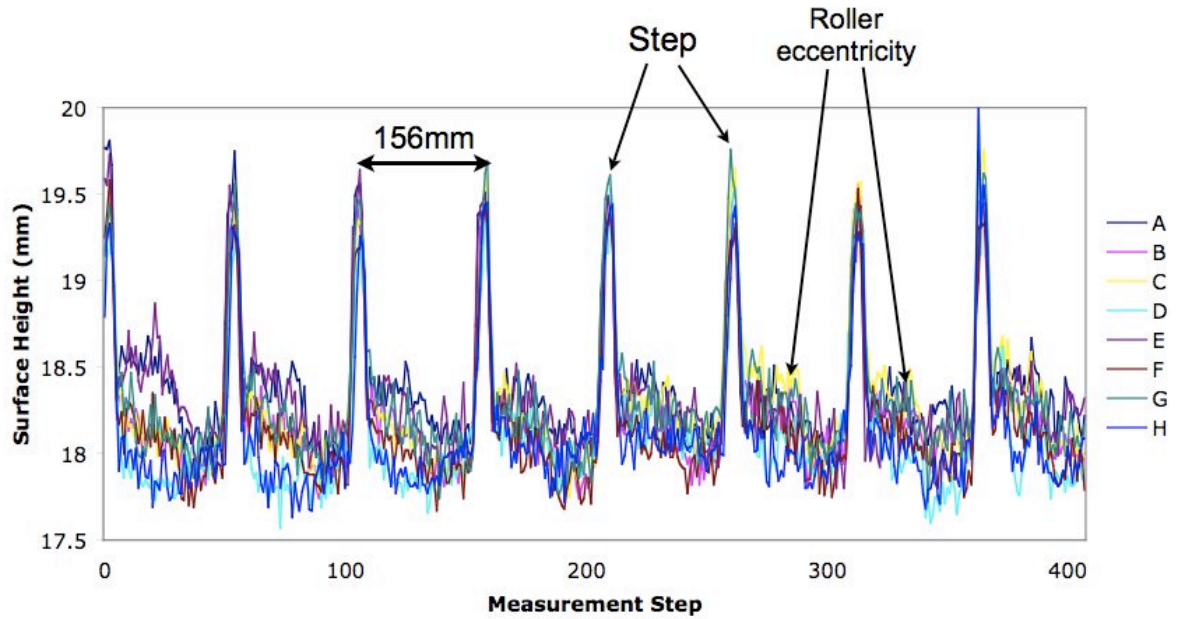


Figure 21: Raw 1-D data for flat board with translational rigid-body motion

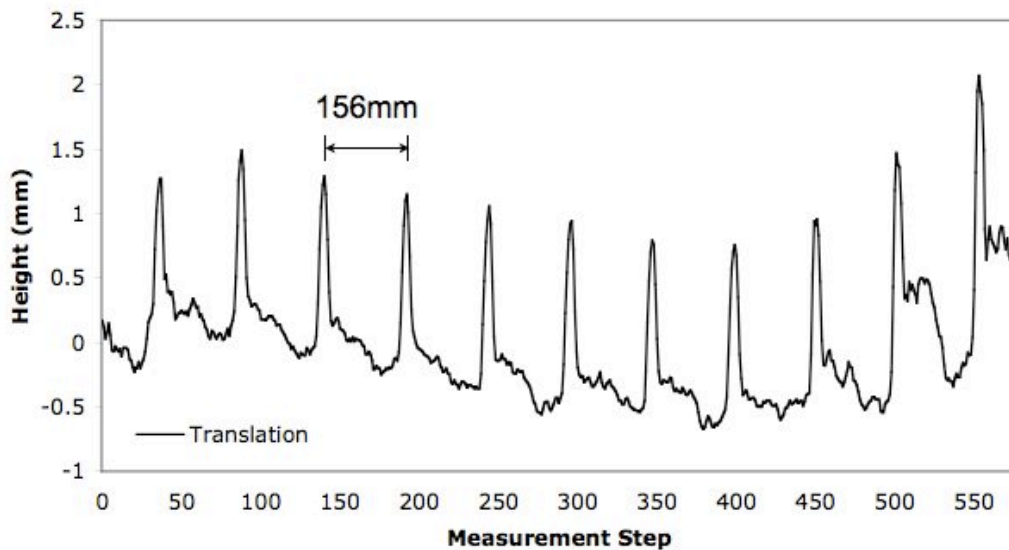


Figure 22: Translation of flat board with step placed on center rollers

The translation shown above is removed from the raw 2-D data leaving a clean 2-D representation of the board surface as shown in Figure 23. It can be seen that the surface has slight curvature indicated by both light blue and red areas. However, this curvature is hardly visible to the naked eye, as it varies within less than 1mm.

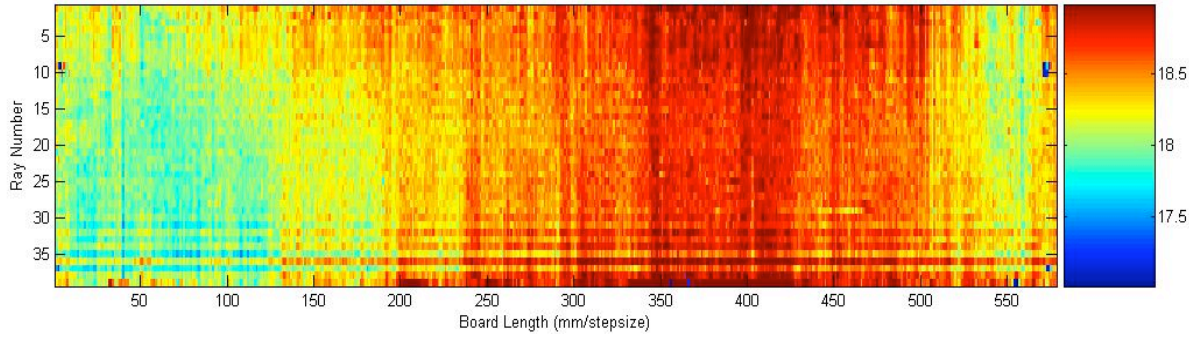


Figure 23: 2-D plot of flat board with translation removed

Figures 24 and 25 are comparison plots between the 1-D recovered profiles u and v and their corresponding u and v -lines in the corrected 2-D data. Data from a single ray in the 2-D corrected data were plotted against the recovered 1-D profiles u and v . The 2-D data are noisy, but they align well with the 1-D recovered profiles. Note that the averages were removed from each set of data in order to align the two sets, as they differ due to boundary conditions set for u and v in the profiling algorithm.

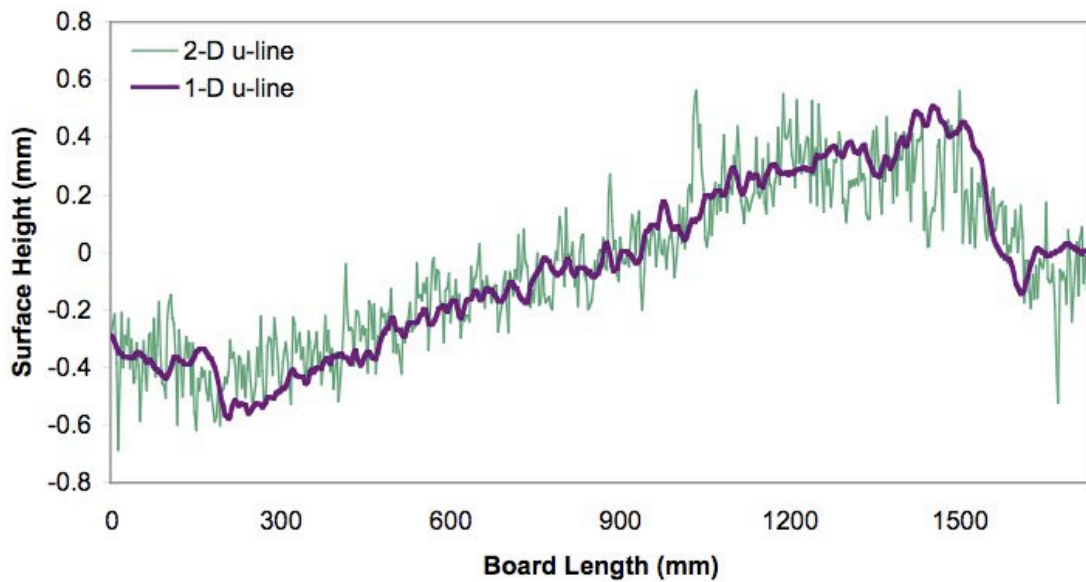


Figure 24: Comparison of 1-D u profile and 2-D u -line profile for flat board

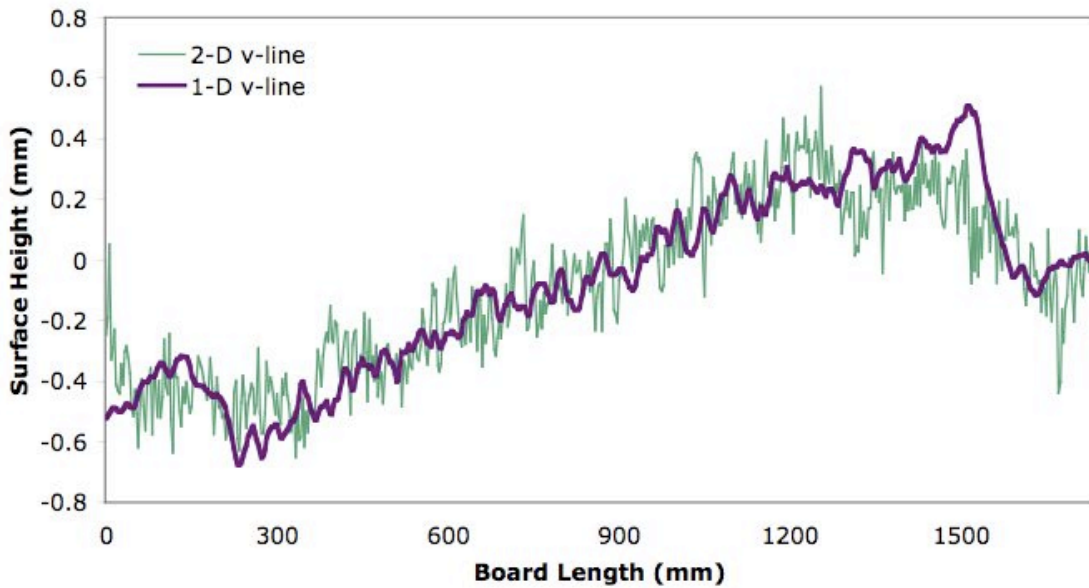


Figure 25: Comparison of 1-D v profile and 2-D v -line profile for flat board

The second case involves measurement of the relatively flat bottom surface of the custom-cut board shown in section 3.3. The sinusoidal surface is in contact with the conveyor rollers causing translation and pitch of the board during measurement. Due to the board's slight twist, roll also occurs. Raw 2-D data for the bottom surface is shown in Figure 26. Consecutive changes in color are visible indicating false height readings due to rigid-body motions.

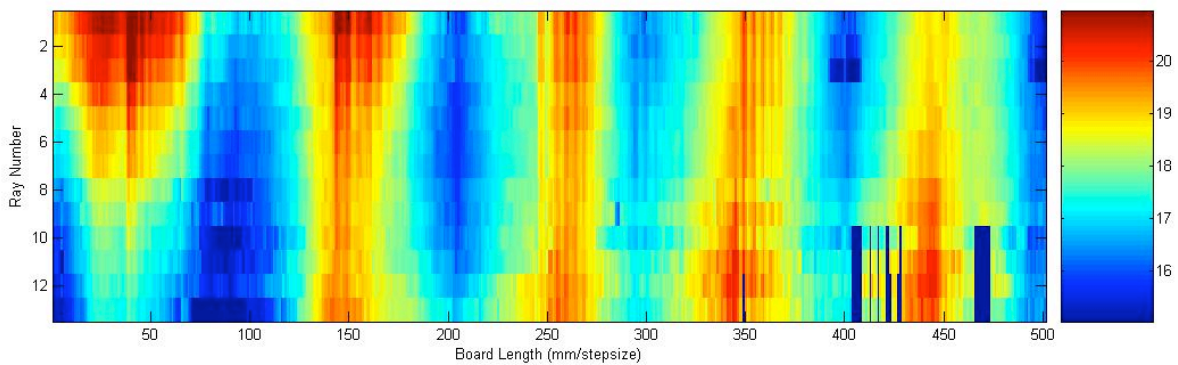


Figure 26: Raw 2-D data for upside-down sinusoidal board

Given that pitch need not be removed from 2-D data, only plots of translation and roll profiles are presented in Figure 27. Again each motion corresponds to a change in color in Figure 26. Each rigid-body motion was removed leaving the actual 2-D representation of the bottom surface as shown in Figure 28.

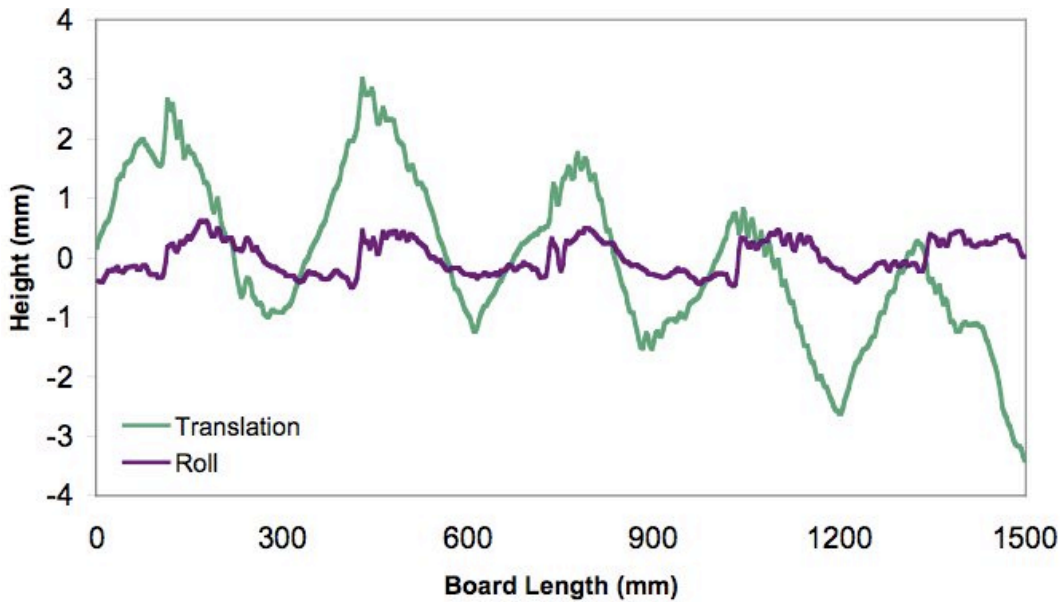


Figure 27: Translation and roll of upside-down snake board

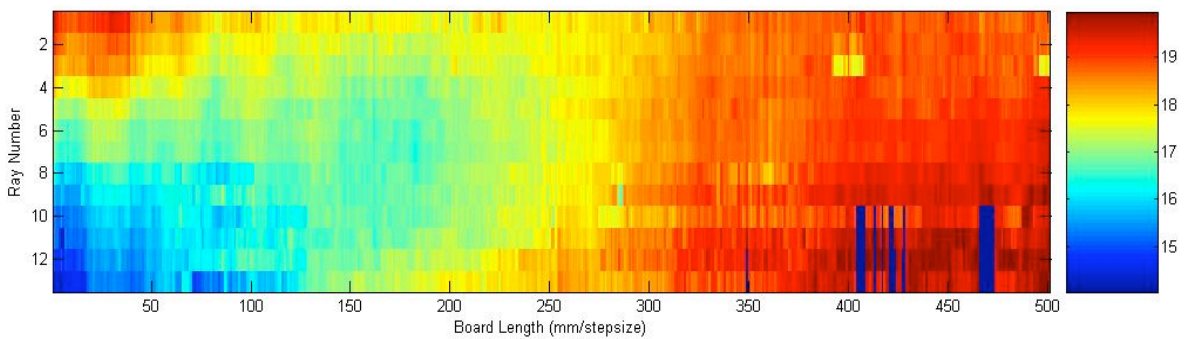


Figure 28: Corrected 2-D plot of bottom surface of sinusoidal board

Board twist and curvature are evidenced by the changes in color corresponding to variations in height on the order of 5mm. Dark blue rectangular areas in the plot indicate

missing data from the line scanner. Figures 29 and 30 show one-dimensional representations of aligned 1-D and 2-D u and v -lines, respectively. The alignment of 2-D u and v -lines to the calculated 1-D u and v profiles indicates that the method for rigid-body motion removal from 2-D data is effective.

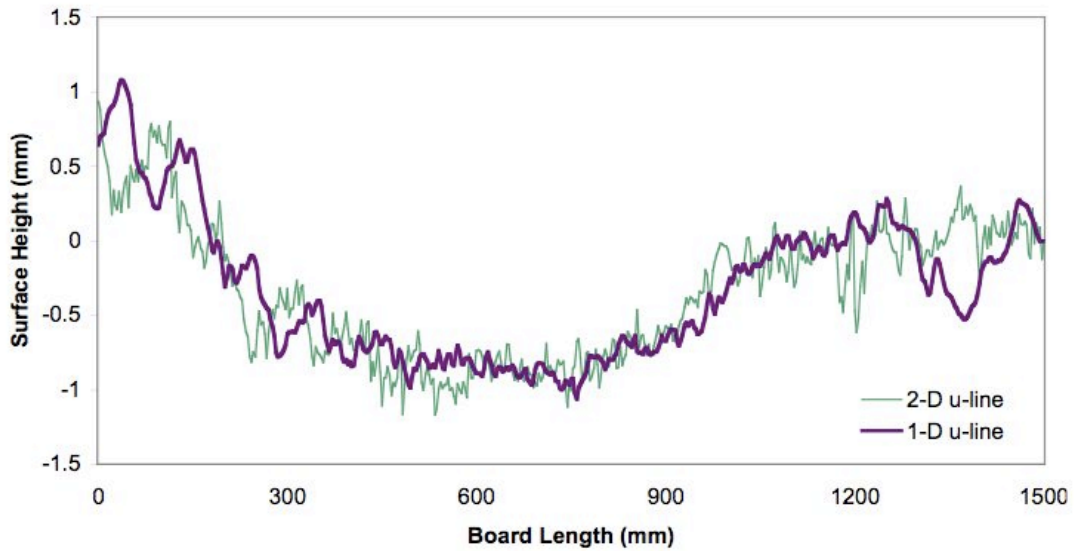


Figure 29: Comparison of 1-D u profile and 2-D u -line profile for upside-down sine board

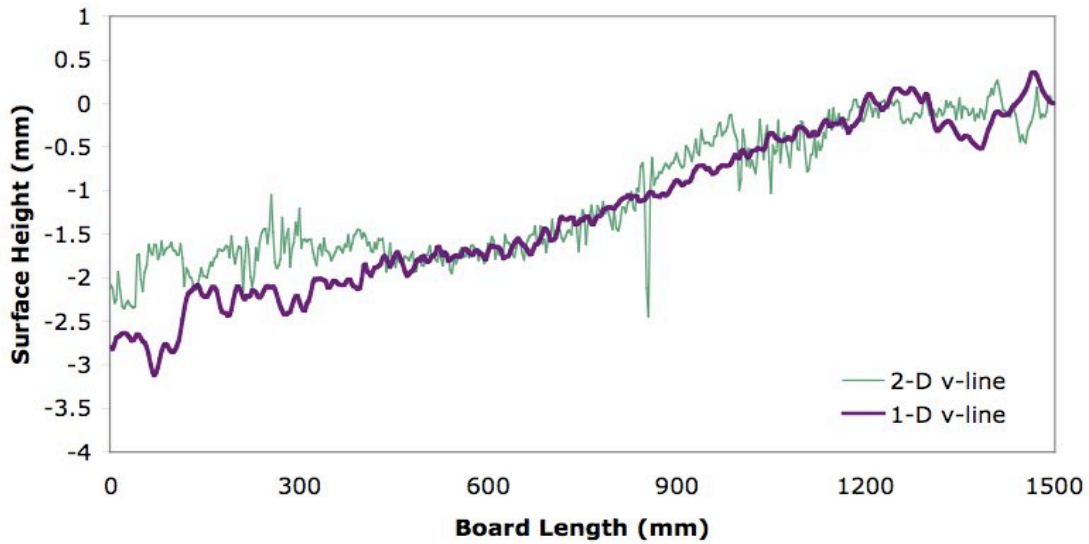


Figure 30: Comparison of 1-D v profile and 2-D v -line profile for upside-down sine board

3.4 Identifying 2-D Surface Features

The following cases demonstrate single-sided 2-D surface profiling of boards with particular surface defects that are of industrial interest with respect to sawmill process control. These defects were unable to be identified using 1-D surface profiling. A 9-sensor (8 point and 1 line) 2-D surface-profiling set-up was used. All spacings were unchanged from the previous two sections.

The first surface of interest contained a washboard defect characterized by a sinusoidal undulation with amplitude of approximately 0.5 to 1mm. In this case, contact with an abnormally vibrating band saw caused a 2-D diagonal pattern across a large part of the board surface. Figure 31 shows the 2-D surface profile of the washboard surface. The diagonal pattern of sinusoidal undulations is indicated by the diagonal stripes of color throughout the length of the board. It can also be seen that this particular surface had a 5mm bow causing the board to slope upwards at the middle.

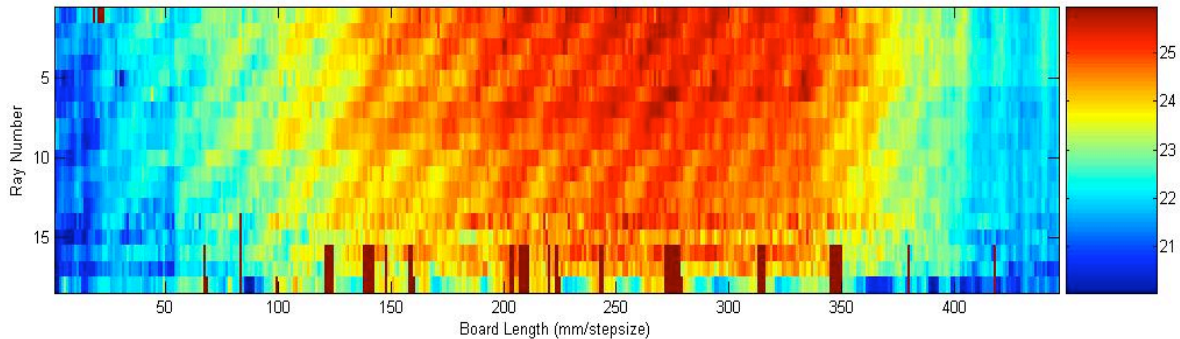


Figure 31: Surface with band saw washboard and 5mm bow

Mismatch surface, also known as step, is another surface defect of interest that is not easily detected by 1-D profiling. It is characterized by a 1-2mm step in the surface running down the length of the board. Mismatch can be caused by poor saw condition such as dull or heated blades, misalignment of saws, or saw instability during cutting [3]. Figure 32 shows

the 2-D surface height profile of a 2"x6" board with a slight step (approximately 1mm) running down the center.

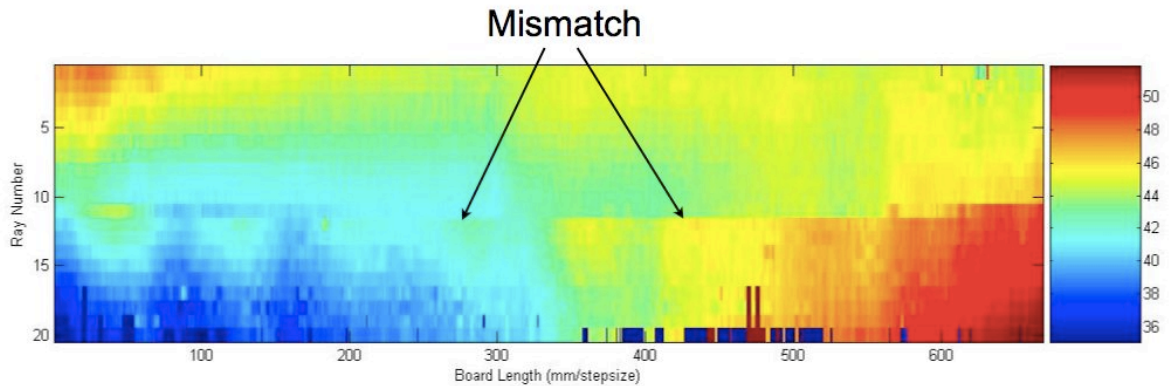


Figure 32: 2"x6" with approximately 1mm step running down center of board

Scallop is a typical chipping-head surface defect. Figure 33 presents the 2-D surface profile of a 2"x10" board with a scallop defect between rays 1 and 10. This board also had a knot tear-out indicated by the dark blue circular area about 150mm from the front of the board between rays 5 and 10. The 1-D parallel-sided sensor arrangement was not able to detect either defect because the sensors did not cover that area of the board.

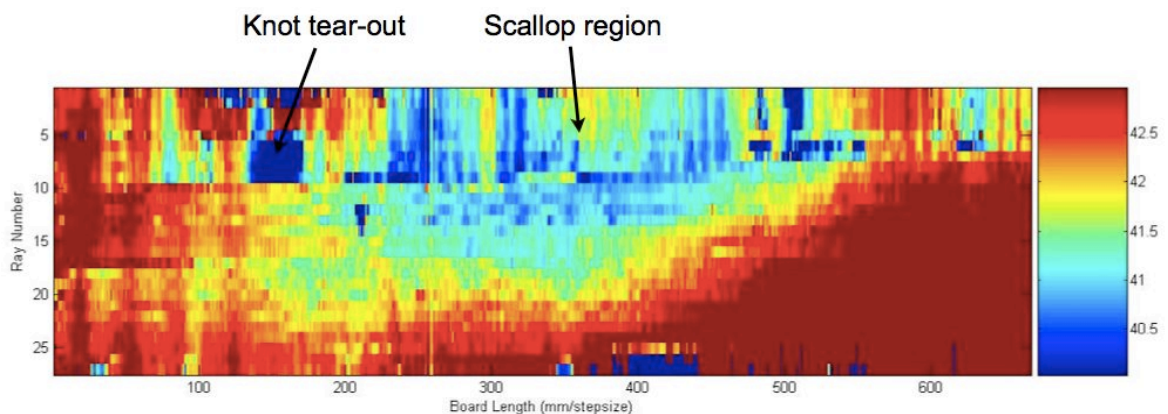


Figure 33: 2"x10" with scallop defect and knot tear-out

Chapter 4: Conclusions

4.1 Summary of Results

Three objectives were defined and achieved in this research work:

1. A 2-D surface profile was obtained for one side of a board completely independent of the opposite side. This was achieved through single-sided measurements taken with both point and line scanners and removal of rigid-body motions from these measurements.

Separate-sided profiling indicates that 2-D surface profiling is better than thickness measurements with regard to enhancing process control. This is because the exact location of a defect on a board can be identified. Given that a different saw or machine typically mills each side of a board, knowing the location of a defect on a board points to the location of a deficiency in the milling process. Adjustments to that machinery component can then be made.

2. The second objective was to obtain an accurate 2-D surface height profile of a lumber board surface that is free of rigid-body motion data contamination. Incorporating the 1-D parallel-sided profiling method allowed identification of translation and roll that were then subtracted from 2-D height data to obtain an accurate 2-D surface profile of the board. Accuracy was approximately 0.3mm.

Two-dimensional surface profiling also contributes more to sawmill process control than 1-D surface profiling because a complete picture of the board is produced. This allows identification of defects anywhere on the surface of the board and identification of defects with specific 2-D patterns. This additional information on each surface of the board aids proper diagnosis of a problem in the milling process.

3. The third objective was to obtain a 2-D surface profile fast enough to keep up with sawmill production speed. Identifying rigid-body motions using a small amount of point laser data instead of a large amount of line laser data helped achieve rapid calculation. Reducing the set of sequential equations to solve for only 1-D surface profiles u and v using Inverse theory also helped reduce calculation time. The time required to produce a 2-D surface profile of a 2.0m board was approximately 0.2 seconds.

4.2 Industrial Implementation

The 2-D surface profiling arrangement is ideally placed immediately after the secondary breakdown in a sawmill where cants are converted into lumber boards for maximum effectiveness in saving raw material. This is where boards are typically sawn oversized to allow for inaccuracies in cutting. Early detection of process deficiencies that cause cutting inaccuracies leads to faster correction of these deficiencies. This diminishes the need to saw boards oversized and diminishes the amount of planing necessary at the end of the milling process. Less valuable fiber is wasted equating to bigger savings in raw material and increased profit for the sawmill.

Laboratory experiments demonstrate that the setup can be readily implemented in a sawmill using off-the-shelf components provided they have at least 1kHz sample rate. Lasers should be positioned as close to the board as possible while remaining in the allowable field of view. This ensures maximum accuracy and reduces the possibility of laser spot displacement due to large vibrations of the setup. The laser setup must also be positioned where boards are singulated and traveling end-to-end with minimal lateral motion.

Eight point sensors and two line lasers produce more accurate results than six point sensors and two line lasers. However, accuracy differs by less than 0.3mm between the 8-sensor and 6-sensor solutions when the sensor arrangement is mounted approximately 680mm from the board surface. Using six sensors instead of eight results in lower initial equipment costs and a marginal sacrifice in accuracy.

4.3 Limitations

Rays are emitted in a fan shape from one side of the line laser (DPS-824), meaning that rays pointing directly below that side of the line laser are vertical and rays that point elsewhere are emitted at an angle. Data loss and extraneous points were frequent, especially at higher conveyor speeds, at the edge of the board opposite the laser source where the ray angle was relatively large. This was especially true in the presence of relatively tall surface features that created shadows that could not be accessed by laser rays. Large roll also contributed to poor edge data as it caused some rays to be activated or partially activated temporarily. This loss of data detracts from the completeness of the 2-D surface height profile, risking loss of surface defect information.

Physical dimensions of the point lasers restrict the spacing between parallel lines to approximately 2.5". This makes it difficult to scan 2"x4" boards and ensure that all lasers are constantly detecting the board surface throughout the entire scan, especially in the presence of roll.

The current parallel-sided profiling arrangement cannot detect side-to-side motion (yaw) of the board during measurement. This may pose difficulties in obtaining an accurate profile of boards in the mill depending on how much yaw they experience.

4.4 Future Work

Adjustments to the line scanner that could result in a reduction of the shadow effect observed in 2-D profiling should be investigated in order to achieve a more reliable complete 2-D profile of the surface.

An alternative bracket design that could position the point lasers closer together should also be investigated to facilitate easier profiling of the common 2"x4" lumber boards.

The current parallel-sided profiling arrangement can be expanded to include sensors that are positioned to measure the sides of the board. This would allow identification of in-plane rigid body translation and pitch (yaw). The additional rigid-body motion information can then be used to adjust the 2-D surface profiles on either side of the board accordingly.

The second line laser can be interfaced with the rest of the system to provide a double-sided 2-D surface profile of a lumber board. This can also provide a 2-D thickness profile as thickness information can be retained with the opposing line scanners. Opportunities for 3-D construction of the board then exist.

End-to-end movement of singulated boards may not be practical in an industrial sawmill, as it requires a large amount of space. Therefore, investigation into 2-D surface profiling of boards moving sideways (edge-to-edge) would provide a better opportunity for direct implementation of the setup in a sawmill.

In order to automate process control, 2-D surface profiles must be interpreted to correctly diagnose a deficiency in the milling process. This constitutes the next stage of work regarding surface profiling of lumber for better sawmill process control.

References

- [1] Lister, P. F., “Results of Sawing Performance Survey in Canadian Softwood Sawmills.” *Project Report No 1215K601*. Forintek Canada Corp, Vancouver, 2005.
- [2] Wong, D., Schajer, G. Personal communication, 2007.
- [3] Rasmussen, H. K., Kozak, R.A., Maness, T.C. “An analysis of machine-caused lumber shape defects in British Columbia Sawmills.” *Forest Products Journal*. Vol. 54, No. 6, pp. 47-56, 2004.
- [4] Maness, T. Lin, Y. “The influence of sawkerf and target size reductions on sawmill revenue and volume recovery”. *Forest Products Journal*. Vol. 45, No. 11/12, pp. 43-50, 1995.
- [5] Schajer, G. S., Gazzarri, J. I., Wong, D. C., Maness, T. C., Kozak, R. A. “Scanner system for separate-sided lumber surface measurements.” *Forest Products Journal*. Vol. 55, No. 12, pp. 173-178, 2005.
- [6] Bennett, J. M. “Review Article: Recent developments in surface roughness characterization.” *Measurement Science and Technology*. Vol. 3, pp. 1119-1127, 1992.
- [7] Corbin, J. “Method and apparatus for measuring surface roughness.” *US Patent 4 573 131*. US Patent and Trademark Office, Washington, 1986.
- [8] Gens, R., Van Genderen, J. L. “Review Article SAR interferometry - issues, techniques, applications.” *International Journal of Remote Sensing*. Vol. 17, No. 10, pp. 1803–1835, 1996.
- [9] Xia, C. C., Yue, Z. Q., Tham, L. G., Lee, C. F., Sun, Z. Q. “Quantifying topography and closure deformation of rock joints.” *International Journal of Rock Mechanics and Mining Sciences*. Vol. 40, pp. 297-220, 2003.
- [10] Bürgmann, R., Rosen, P., Fielding, E. “Synthetic Aperture Radar Interferometry to Measure Earth’s Surface Topography and Its Deformation.” *Annual Review of Earth and Planetary Sciences*. Vol. 28, pp. 169-209, 2000.
- [11] Stevens, D. R., Cumming, I. G., Gray, A. L. “Options for Airborne Interferometric SAR Motion Compensation.” *IEEE Transactions on Geoscience and Remote Sensing*. Vol. 33, No. 2, pp. 409-420, 1995.
- [12] Hudson, W. “High speed road profile equipment evaluation.” *Highway Research Record*. National Research Council, Highway Research Board. Vol. 189, pp. 150-165, 1967.

- [13] Darlington, J. "A progress report on the evaluation and application study of the General Motors Rapid Travel Road Profilometer." *Highway Research Record*. National Research Council, Highway Research Board. Vol. 214, pp. 50-67, 1968.
- [14] Takeshita, K. "A method for track irregularity inspection by asymmetrical chord offset method". *Quarterly Report of RTRI*. Railway Technical Research Institute. Vol. 33, No. 2, pp. 106-114, 1992.
- [15] Cooper, J. "Rail Corrugation Measurement." *Proceedings of "Rail Technology"*, Nottingham, UK. (eds. C. O. Frederick and D. J. Round). pp.207-223, Sept. 21-29, 1981.
- [16] Gazzarri, J. I. "Sequential Measurements Method for Moving Surfaces Profiling." M.A.Sc. Thesis: Department of Mechanical Engineering. University of British Columbia, 2003.
- [17] Schajer, G. S., Gazzarri, J. I. "Surface Profiling Using Sequential Sampling and Inverse Methods. Part I: Mathematical Background." *Experimental Mechanics*. Vol. 44, No. 5, pp. 473-479, 2004.
- [18] Boccione, M., Caprioli, A., Cigada, A., Collina, A. "A measurement system for quick rail inspection and effective track maintenance strategy." *Mechanical Systems and Signal Processing*. Vol. 21, No. 3, pp. 1242-1254, 2007.
- [19] Gazzarri, J., Schajer, G. "Lumber surface profiling independent of bulk motion." *Holz als Roh- und Werkstoff*. Vol. 63, No. 5, pp. 347-352, 2005.
- [20] Schajer, G. S., Gazzarri, J. I. "Surface Profiling Using Sequential Sampling and Inverse Methods. Part II: Implementation and Experimental Results." *Experimental Mechanics*. Vol. 44, No. 5, pp. 480-485, 2004.
- [21] Scales, J., Smith, M., Treitel, S. "Introductory Geophysical Inverse Theory." *Samizdat Press*. Center for Wave Phenomena. Dept. Geophysics, Colorado School of Mines, 2001.
- [22] Tikhonov, A., Goncharsky, A., Stepanov, V., Yagola, A. "Numerical Methods for the Solution of Ill-Posed Problems." Kluwer, Dordrecht, 1995.
- [23] Tikhonov, A., Arsenin, V. "Solutions of ill-posed problems". John Wiley & Sons, Washington, D. C. 1977.

[24] Marchand, P., Marmet, L. "Binomial smoothing filter: A way to avoid some pitfalls of least-squares polynomial smoothing." *Review of Scientific Instruments*. Vol. 54, No. 8, pp. 1034-1041, 1983.

[25] Schajer, G.S. "Hole-Drilling Residual Stress Profiling With Automated Smoothing." *Journal of Engineering Materials and Technology*. Vol. 129, pp. 440-445, 2007.